



## **Modelling land-atmosphere daily exchanges of NO, NH<sub>3</sub>, and CO<sub>2</sub> in a semi-arid grazed ecosystem in Senegal**

Delon, Claire; Galy-Lacaux, Corinne; Serca, Dominique; Personne, Erwan; Mougin, Eric; Adon, Marcellin; Le Dantec, Valerie; Loubet, Benjamin; Fensholt, Rasmus; Tagesson, Torbern

*Published in:*  
Biogeosciences

*DOI:*  
[10.5194/bg-16-2049-2019](https://doi.org/10.5194/bg-16-2049-2019)

*Publication date:*  
2019

*Document version*  
Publisher's PDF, also known as Version of record

*Document license:*  
[CC BY](#)

*Citation for published version (APA):*  
Delon, C., Galy-Lacaux, C., Serca, D., Personne, E., Mougin, E., Adon, M., ... Tagesson, T. (2019). Modelling land-atmosphere daily exchanges of NO, NH<sub>3</sub>, and CO<sub>2</sub> in a semi-arid grazed ecosystem in Senegal. *Biogeosciences*, 16(9), 2049-2077. <https://doi.org/10.5194/bg-16-2049-2019>



# Modelling land–atmosphere daily exchanges of NO, NH<sub>3</sub>, and CO<sub>2</sub> in a semi-arid grazed ecosystem in Senegal

Claire Delon<sup>1</sup>, Corinne Galy-Lacaux<sup>1</sup>, Dominique Serça<sup>1</sup>, Erwan Personne<sup>2</sup>, Eric Mougin<sup>3</sup>, Marcellin Adon<sup>1,6</sup>, Valérie Le Dantec<sup>4</sup>, Benjamin Loubet<sup>2</sup>, Rasmus Fensholt<sup>5</sup>, and Torbern Tagesson<sup>5</sup>

<sup>1</sup>Laboratoire d'Aérodynamique, Université de Toulouse, CNRS, UPS, Toulouse, France

<sup>2</sup>UMR ECOSYS, INRA, AgroParisTech, Université Paris-Saclay, 78850, Thiverval-Grignon, France

<sup>3</sup>Géosciences Environnement Toulouse, Université de Toulouse, CNES, CNRS, IRD, UPS, Toulouse, France

<sup>4</sup>Centre d'Etudes Spatiales de la Biosphère, Université de Toulouse, CNES, CNRS, IRD, UPS, Toulouse, France

<sup>5</sup>Department of Geosciences and Natural Resource Management, University of Copenhagen, Copenhagen, Denmark

<sup>6</sup>Laboratoire de Physique de l'Atmosphère, et de Mécanique des Fluides, Université Félix Houphouët-Boigny, Abidjan, Côte d'Ivoire

**Correspondence:** Claire Delon (claire.delon@aero.obs-mip.fr)

Received: 30 July 2018 – Discussion started: 27 August 2018

Revised: 19 April 2019 – Accepted: 24 April 2019 – Published: 15 May 2019

**Abstract.** Three different models (STEP–GENDEC–NOflux, Zhang2010, and Surfalm) are used to simulate NO, CO<sub>2</sub>, and NH<sub>3</sub> fluxes at the daily scale for 2 years (2012–2013) in a semi-arid grazed ecosystem at Dahra (15°24'10" N, 15°25'56" W, Senegal, Sahel). Model results are evaluated against experimental results acquired during three field campaigns. At the end of the dry season, when the first rains re-wet the dry soils, the model STEP–GENDEC–NOflux simulates the sudden mineralization of buried litter, leading to pulses in soil respiration and NO fluxes. The contribution of wet season fluxes of NO and CO<sub>2</sub> to the annual mean is respectively 51 % and 57 %. NH<sub>3</sub> fluxes are simulated by two models: Surfalm and Zhang2010. During the wet season, air humidity and soil moisture increase, leading to a transition between low soil NH<sub>3</sub> emissions (which dominate during the dry months) and large NH<sub>3</sub> deposition on vegetation during wet months. Results show a great impact of the soil emission potential, a difference in the deposition processes on the soil and the vegetation between the two models with however a close agreement of the total fluxes. The order of magnitude of NO, NH<sub>3</sub>, and CO<sub>2</sub> fluxes is correctly represented by the models, as well as the sharp transitions between seasons, specific to the Sahel region. The role of soil moisture in flux magnitude is highlighted, whereas the role of soil temperature is less obvious. The simultaneous increase in NO and CO<sub>2</sub> emissions and NH<sub>3</sub>

deposition at the beginning of the wet season is attributed to the availability of mineral nitrogen in the soil and also to microbial processes, which distribute the roles between respiration (CO<sub>2</sub> emissions), nitrification (NO emissions), volatilization, and deposition (NH<sub>3</sub> emission/deposition). The objectives of this study are to understand the origin of carbon and nitrogen compounds exchanges between the soil and the atmosphere and to quantify these exchanges on a longer timescale when only a few measurements have been performed.

## 1 Introduction

The Sahel is one of the largest semi-arid regions in the world and it is a transition zone between the Sahara desert in the north and the more humid Sudanese savanna in the south. In semi-arid zones, the exchanges of trace gases are strongly influenced by hydrologic pulses defined as temporary increases in water inputs (Harms et al., 2012). In the West African Sahel (between 12° N/18° N, 15° W/10° E), soil water availability strongly affects microbial and biogeochemical processes in all ecosystem compartments (Wang et al., 2015), which in turn determines the exchange fluxes of C and N (Austin et al., 2004; Tagesson et al., 2015a; Shen et al., 2016). After a long dry period (8 to 10 months in the Sa-

hel), the first rainfall events of the wet season cause strong pulses of  $\text{CO}_2$ ,  $\text{N}_2\text{O}$ ,  $\text{NO}$ , and  $\text{NH}_3$  to the atmosphere (Jaeglé et al., 2004; McCalley and Sparks, 2008; Delon et al., 2015; Shen et al., 2016; Tagesson et al., 2016b). Anthropogenic activities have a strong impact on N and C cycling, and in large parts of the world, deposition of N compounds has several damaging impacts on ecosystem functions, such as changes in species biodiversity (Bobbink et al., 2010). The Sahel is still a protected region from this N pollution (Bobbink et al., 2010), but climate change could create an imbalance in biogeochemical cycles of nutrients (Delgado-Baquerizo et al., 2013).

The emission of  $\text{NO}$  from soils leads to the formation of  $\text{N}_2\text{O}$  and  $\text{O}_3$  in the troposphere. Soil  $\text{NO}$  biogenic emissions from the African continent expressed in teragrammes of nitrogen per year are considered as the largest in the world (Fowler et al., 2015) because of extended natural areas. The pulses of  $\text{NO}$  from the Sahel region at the beginning of the wet season have been shown to strongly influence the overlying  $\text{N}_2\text{O}$  tropospheric column (Jaeglé et al., 2004; Hudman et al., 2012; Zörner et al., 2016), indicating the urgent need for improved understanding of the dynamics of  $\text{NO}$  pulses from this region.  $\text{NH}_3$  emissions lead to the formation of particles in the atmosphere, such as ammonium nitrates ( $\text{NH}_4\text{NO}_3$ ), whose vapour phase dissociation further produces  $\text{NH}_3$  and  $\text{HNO}_3$  (Fowler et al., 2015). The land–atmosphere exchange of ammonia varies in time and space depending on environmental factors such as climatic variables, soil energy balance, soil characteristics, and plant phenology (Flechard et al., 2013). Emissions of these compounds involve changes in atmospheric composition (ozone and aerosol production) and effects on climate through greenhouse gas impacts.

The N exchange fluxes are also influenced by the soil N content, and the main inputs of N compounds into the soil in semi-arid uncultivated regions are biological nitrogen fixation (BNF), decomposition of organic matter (OM), and atmospheric wet and dry deposition (Perroni-Ventura et al., 2010). Soil N losses to the atmosphere involve  $\text{N}_2\text{O}$ ,  $\text{NH}_3$ , and  $\text{NO}$  gaseous emissions, whereas within the soil, N can be lost via erosion, leaching, and denitrification.  $\text{NO}$  emissions to the atmosphere are mainly the result of nitrification processes, which is the oxidation of  $\text{NH}_4^+$  to nitrates ( $\text{NO}_3^-$ ) via nitrites ( $\text{NO}_2^-$ ) through microbial processes (Pilegaard et al., 2013; Conrad, 1996). In remote areas, where anthropogenic emissions such as industrial or traffic pollution do not happen,  $\text{NH}_3$  bidirectional exchanges are regulated through diverse processes:  $\text{NH}_3$  is emitted by livestock excreta, soil, and litter and is regulated by the availability of  $\text{NH}_4^+$  and  $\text{NH}_3$  in the aqueous phase ( $\text{NH}_x$ ), by the rate of mineralization of  $\text{NH}_4^+$ , and by the availability of water, which allows  $\text{NH}_x$  to be dissolved, to be taken up by organisms, and to be released through decomposition (Schlesinger et al., 1991; Sutton et al., 2013). Additionally  $\text{NH}_3$  can be dry and wet deposited on soil and litter (Laouali et al., 2012; Vet et al., 2014), leaf cuticles, and stomata and regulated by chemical

interactions within the canopy air space (Loubet et al., 2012). The N cycle is closely linked to the C cycle, and it has been suggested that C–N interactions may regulate N availability in the soil (Perroni-Ventura et al., 2010). The link between N and C cycles in the soil, and their effects on OM decomposition, affect the emissions of C and N compounds to the atmosphere. These cycles are interlinked by respiration and decomposition processes in the soil, and the balance between C and N is controlled by biological activity, mainly driven by water availability in drylands (Delgado-Baquerizo et al., 2013). Indeed, the decomposition of soil OM, and its efficiency, regulates the amount of  $\text{CO}_2$  that is released to the atmosphere (Elberling et al., 2003).

Biogeochemical regional models have been applied for N compound emissions mostly in temperate regions (Butterbach-Bahl et al., 2001, 2009), where the spatial and temporal resolution of data is well characterized. Global approaches have also been developed, with a simplified description of processes and with coarse spatial resolution (Yienger and Levy, 1995; Potter et al., 1996; Yan et al., 2005; Hudman et al., 2012). Considering the weak number of experimental data in semi-arid regions about trace gas exchanges and their driving parameters, one-dimensional modelling is a complementary, essential, and alternative way of studying the annual cycle dynamics and the underlying processes of emission and deposition. The specificity of the semi-arid climate needs to be precisely addressed in the models used to be able to correctly represent the pulses of emissions and the strong changes in C and N dynamics at the transition between seasons. Improving the description of processes in 1-D models in tropical regions is therefore a necessary step before implementing regional modelling.

In this study, three main modelling objectives are focused on (1) investigating the links between N and C cycles in the soil and consecutive daily exchanges of  $\text{NO}$ ,  $\text{NH}_3$ , and  $\text{CO}_2$  between the soil and the atmosphere, at the annual scale and specifically at the transition between seasons, (2) comparing two different formalisms for  $\text{NH}_3$  bidirectional exchange, and (3) highlighting the influences of environmental parameters on these exchanges. Different one-dimensional models, specifically developed or adapted for semi-arid regions, were used in the study. As a study site, representative of the semi-arid region of the western Sahel, we selected the Dahra field site located in the Ferlo region of Senegal (Tagesson et al., 2015b). The one-dimensional models were applied for the years 2012 and 2013 to simulate the land–atmosphere exchange fluxes of  $\text{CO}_2$ ,  $\text{NO}$ , and  $\text{NH}_3$ . Model results were compared to flux measurements collected during three field campaigns in Dahra in July 2012 (7 d), July 2013 (8 d), and November 2013 (10 d), and presented in Delon et al. (2017).

## 2 Materials and methods

### 2.1 Field site

Measurements were performed at the Dahra field station, part of the Centre de Recherches Zootechniques (CRZ), in the Sahelian region of Ferlo, Senegal ( $15^{\circ}24'10''$  N,  $15^{\circ}25'56''$  W). The Dahra field site is located within the CRZ managed by the Institut Sénégalais de Recherche Agronomique (ISRA). This site is a semi-arid savanna used as a grazed rangeland. The Sahel is under the influence of the West African Monsoon (cool wet southwesterly wind) and the Harmattan (hot dry northeasterly wind) depending on the season. Rainfall is concentrated in the core of the monsoon season, which extends from mid-July to mid-October. At Dahra, the annual rainfall was 515 mm in 2012 and 356 mm in 2013 with an average of 416 mm for the period 1951–2013. The annual mean air temperature at 2 m height was  $28.4^{\circ}\text{C}$  in 2012 and  $28.7^{\circ}\text{C}$  in 2013, with an average of  $29^{\circ}\text{C}$  for the period 1951–2003. The most abundant tree species are *Balanites aegyptiaca* and *Acacia tortilis*, and the herbaceous vegetation is dominated by annual  $\text{C}_4$  grasses (e.g. *Dactyloctenium aegyptium*, *Aristida adscensionis*, *Cenchrus biflorus*, and *Eragrostis tremula*) (Tagesson et al., 2015a). Livestock is dominated by cows, sheep, and goats, and grazing occurs permanently all year-round (Assouma et al., 2017). This site was previously described in Tagesson et al. (2015b) and Delon et al. (2017).

### 2.2 Field data

#### 2.2.1 Hydro-meteorological data and sensible and latent heat fluxes

A range of hydro-meteorological variables are measured by a meteorological station at the Dahra field site (Tagesson et al., 2015b). The hydro-meteorological variables used in this study were rainfall (mm), air temperature ( $^{\circ}\text{C}$ ), relative air humidity (%), wind speed ( $\text{m s}^{-1}$ ), air pressure (hPa) at 2 m height, soil temperature ( $^{\circ}\text{C}$ ), soil moisture (%) at 0.05, 0.10, and 0.30 m depth, and net radiation ( $\text{W m}^{-2}$ ). Data were sampled every 30 s and stored as 15 min averages (sum for rainfall). Data have then been 3 h and daily averaged for the purpose of this study.

Land–atmosphere exchanges of sensible and latent heat was measured for the years 2012 and 2013 with an eddy covariance system consisting of an open-path infrared gas analyzer (LI-7500, LI-COR Inc., Lincoln, USA) and a three-axis sonic anemometer (Gill R3 ultrasonic anemometer, Hampshire, UK) (Tagesson et al., 2015a). The sensors were mounted 9 m above the ground and data were collected at a 20 Hz rate. The post-processing was performed with the EddyPro 4.2.1 software (LI-COR Biosciences, 2012) and statistics were calculated for 30 min periods. For a thorough de-

scription of the post-processing of sensible and latent heat fluxes, see Supplement of Tagesson et al. (2015b).

#### 2.2.2 Atmospheric $\text{NH}_3$ concentrations using passive samplers

Atmospheric concentrations of  $\text{NH}_3$  and other compounds such as  $\text{N}_2\text{O}$ ,  $\text{HNO}_3$ ,  $\text{O}_3$ , and  $\text{SO}_2$  were measured using passive samplers on a monthly basis, in accordance with the methodology used within the INDAAF (International Network to study Deposition and Atmospheric chemistry in Africa) program (<https://indaaf.obs-mip.fr>, last access: 8 May 2019) driven by the Laboratoire d'Aerologie (LA) in Toulouse. While not being actually part of the INDAAF network, the Dahra site was equipped with the same passive sampler devices and analyses of these samplers were performed following the INDAAF protocol at LA.

Passive samplers were mounted under a stainless-steel holder to avoid direct impact from wind transport and splashing from precipitation. The holder was attached at a height of about 1.5 m above ground. All the samplers were exposed in pairs in order to ensure the reproducibility of results. The samplers were prepared at LA in Toulouse, installed and collected after 1 month exposure by a local investigator, and sent back to LA. Samplers before and after exposition were stored in a fridge ( $4^{\circ}\text{C}$ ) to minimize possible bacterial decomposition or other chemical reactions. Samplers were then analysed by ion chromatography (IC) to determine ammonium and nitrate concentrations. Validation and quality control of passive samplers according to international standards (World Meteorological Organization report), as well as the sampling procedure and chemical analysis of samples, have been widely detailed in Adon et al. (2010). Monthly mean  $\text{NH}_3$  concentrations in parts per billion by volume are calculated for the period 2012 and 2013. The measurement accuracy of  $\text{NH}_3$  passive samplers, evaluated through covariance with duplicates, and the detection limit evaluated from field blanks were estimated respectively at 14 % and  $0.7 \pm 0.2$  ppb (Adon et al., 2010).

#### 2.2.3 Measurements of $\text{NO}$ , $\text{NH}_3$ , and $\text{CO}_2$ (respiration) fluxes from soil and soil physical parameters

$\text{NO}$ ,  $\text{NH}_3$ , and  $\text{CO}_2$  fluxes were measured for 7 d in July 2012, 8 d in July 2013, and 10 d in November 2013; these periods will hereafter be called J12, J13, and N13 respectively. The samples were taken at three different locations along a 500 m transect following a weak dune slope (top, middle, and bottom) with one location per day. Each location was then sampled every 3 d, approximately from 08:00 to 19:00 UTC for soil fluxes, and 24 h a day for  $\text{NO}$  and  $\text{NH}_3$  concentrations. Between 15 and 20 fluxes were measured each day during the three campaigns.

NO and NH<sub>3</sub> fluxes were measured with a manual closed dynamic Teflon chamber (non-steady-state through-flow chamber; Pumpanen et al., 2004) with dimensions of 200 mm width × 400 mm length × 200 mm height. During the J12 campaign, the chamber was connected to a Laboratoire d'Aerologie analyzer, whereas in J13 and N13, it was connected to a Thermo Scientific 17I analyzer (ThermoFischer Scientific, MA, USA). The calculation of fluxes is based on an equation detailed in Delon et al. (2017), adapted from Davidson et al. (1991). The increase rate of NO and NH<sub>3</sub> mixing ratios used in the flux calculation equation was estimated by a linear regression fitted to data measured for 180 to 300 s for NO (120 s for NH<sub>3</sub>) following the installation of the chamber on the soil, as detailed in Delon et al. (2017). Close to the Teflon chamber, soil CO<sub>2</sub> respiration was measured with a manual closed dynamic chamber (SRC-1 from PP Systems, 150 mm height × 100 mm diameter) coupled to a non-dispersive infrared CO<sub>2</sub>/H<sub>2</sub>O analyzer EGM-4 (PP Systems, Hitchin, Hertfordshire, UK). Soil CO<sub>2</sub> respiration was measured within 30 cm of the location of the NO and NH<sub>3</sub> fluxes. Measurements were performed on bare soil to ensure only root and microbe respiration. Results of NO, NH<sub>3</sub>, and CO<sub>2</sub> fluxes are presented as daily means with daily standard deviations. Along with flux measurements, soil physical parameters were measured during the campaigns: soil pH ranges from 5.77 to 7.43, sand content ranges between 86 % and 94 %, and clay content ranges between 4.7 % and 7.9 %. All the methods, calculations, and results from the field campaigns are fully detailed in Delon et al. (2017).

### 2.3 Modelling biogenic NO fluxes, CO<sub>2</sub> respiration, and ammonium content in STEP–GENDEC–NOflux

#### 2.3.1 The STEP–GENDEC model

The STEP model is presented in Appendix A, with forcing variables detailed in Table A1, site parameters used in the initialization in Table A2, numerical values of parameters used in the equations in Table A3, and equations, variables, parameters, and constants used in the equations in Table A4.

STEP is an ecosystem process model for Sahelian herbaceous savannas (Mougin et al., 1995; Tracol et al., 2006; Delon et al., 2015). It is coupled to GENDEC, which aims at representing the interactions between litter, decomposer microorganisms, microbial dynamics, and C and N pools (Moorhead and Reynolds, 1991). It simulates the decomposition of the organic matter and microbial processes in the soil in arid ecosystems. Information such as the quantity of organic matter from faecal matter from livestock and herbal masses is transferred from STEP as inputs to GENDEC (Fig. 1).

Soil temperatures are simulated from air temperature according to Parton (1984). This model requires daily maximal and minimal air temperature, global radiation (provided by

forcing data), herbaceous aboveground biomass (provided by the model), initial soil temperature, and soil thermal diffusivity. Details of equations are given in Delon et al. (2015) and Appendix A (Tables A3 and A4).

Soil moisture values are calculated following the tipping-bucket approach (Manabe, 1969): when the field capacity is reached, the excess water in the first layer (0–2 cm) is transferred to the second layer, between 2 and 30 cm. Two other layers are defined, between 30–100 cm and 100–300 cm. Equations related to soil moisture calculation are detailed in Appendix A (Table A4) and in Jarlan et al. (2008). This approach, while being simple in its formulation, is especially useful in regions where detailed description of the environment is not available or unknown, and where the natural heterogeneity of the soil profile is high due to the presence of diverse matter fragments such as buried litter, dead roots from herbaceous mass and trees, stones, branches, and tunnels dug by insects and little mammals.

The STEP model is forced daily by rain, global radiation, air temperature, wind speed, and relative air humidity at 2 m height. Initial parameters specific to the Dahra site are listed in Table A1 and site parameters in Table A2.

#### 2.3.2 Respiration and biogenic NO fluxes

The quantity of carbon in the soil was calculated from the total litter input from faecal and herbal mass, where faecal matter is obtained from the number of livestock heads grazing at the site (Diawara, 2015; Diawara et al., 2018). The quantity of carbon is 50 % the buried litter mass. The carbon and nitrogen exchanges between pools and all equations are detailed in Moorhead and Reynolds (1991) and will not be developed here. Carbon dynamics depend on soil temperature, soil moisture, and soil nitrogen (linked to microbial dynamics). The concentration of nitrogen in the soil is derived from the quantity of carbon using C/N ratios.

Biogenic NO fluxes were calculated using the coupled model STEP–GENDEC–NOflux, as detailed in Delon et al. (2015). The NOflux model uses an artificial neural network approach to estimate the biogenic NO emission from soil to the atmosphere (Delon et al., 2007, 2015). The NO flux is calculated from and depends on parameters such as soil surface temperature and moisture, soil temperature at 30 cm depth, sand percentage, N input (here given as a percentage of the ammonium content in the soil), wind speed, and soil pH. The input of N to the soil from the buried litter is provided by STEP, and the calculation of the ammonium content in the soil coming out from this N input is provided by GENDEC. The equations used for NO flux calculation are reported in Appendix B, taken from Delon et al. (2015).

The main structure of the model is kept identical as in the Delon et al. (2015) version, except for N uptake by plants, for which the present paper proposes a formulation detailed in Appendix C. In brief, in the previous version of the model 2 % of the NH<sub>4</sub><sup>+</sup> pool of the soil was used for NO emission

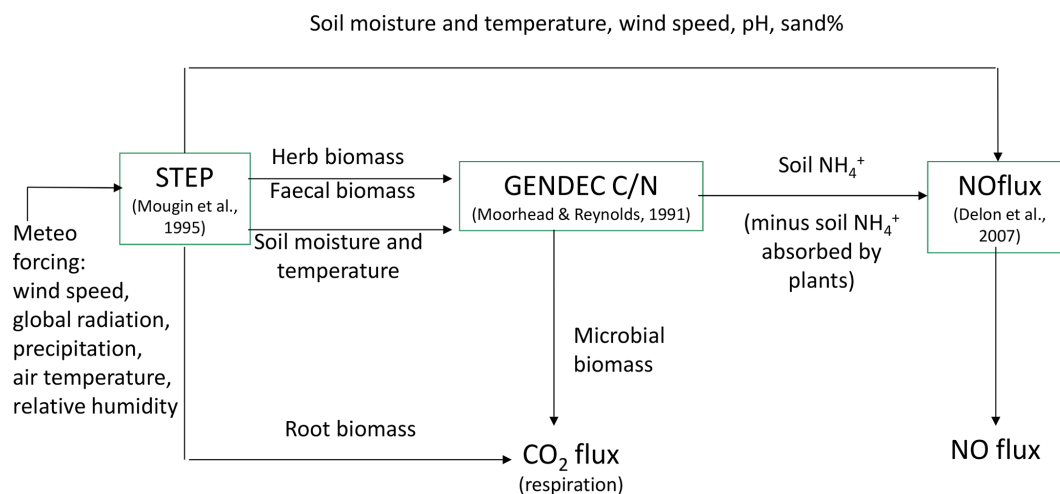


**Figure 1.** Schematic representation of NO and CO<sub>2</sub> flux modelling in STEP–GENDEC–NOflux (adapted from Delon et al., 2015).

calculation. In the current version, the NO emitted to the atmosphere results from 1 % of the  $\text{NH}_4^+$  pool in the soil minus the N absorbed by plants. The percentage of soil  $\text{NH}_4^+$  pool used to calculate the NO emission has been changed from 2 % to 1 % based on Potter et al. (1996), who proposed a range between 0.5 % and 2 %. In the present study, the 1 % value was more adapted to fit experimental values.

Soil respiration is the sum of autotrophic (root only) and heterotrophic respiration. The autotrophic respiration in STEP is calculated from growth and maintenance respirations of roots and shoots (Mougin et al., 1995), following equations reported in Table A4. Autotrophic respiration depends on root depth soil moisture and soil temperature (2–30 cm) and root biomass, whose dynamics are simulated by STEP. The heterotrophic respiration is calculated in GENDEC from the growth and death of soil microbes in the soil depending on the available litter C (given by STEP). Microbial respiration  $\rho$  in grammes of carbon per day is calculated as in Eq. (1).

$$\rho = (1 - \varepsilon)\text{Ca} \quad (1)$$

Microbial growth in grammes of carbon per day is  $\gamma = \varepsilon \text{Ca}$ , where  $\varepsilon$  is the assimilation efficiency (unitless) and Ca is total C available in grammes of carbon per day, i.e. total C losses from four different litter inputs, buried litter, litter from trees, faecal matter, and dry roots. Microbial death is driven by the death of the living microbe mass, and the change in water potential during drying–wetting cycles (change between  $-1.5$  and  $-0.01$  MPa in the layer 2–30 cm). These calculations are described in Moorhead and Reynolds (1991) and Delon et al. (2015) and are not reported in detail in this study. A schematic view of STEP–GENDEC–NOflux is presented in Fig. 1. Simulated variables and corresponding measurements used for validation are summarized in Table 1.

## 2.4 Modelling NH<sub>3</sub> fluxes

The net NH<sub>3</sub> flux between the surface and the atmosphere depends on the concentration difference  $\chi_{\text{cp}} - C_{\text{NH}_3}$ , where  $C_{\text{NH}_3}$  is the ambient NH<sub>3</sub> concentration in microgrammes per cubic metre, and  $\chi_{\text{cp}}$  is the concentration of the canopy compensation point in microgrammes per cubic metre. The canopy compensation point concentration is the atmospheric NH<sub>3</sub> concentration in the canopy for which the fluxes between the soil, the stomatal cavities, and the air inside the canopy switch from emission to deposition, or vice versa (Farquhar et al., 1980; Wichink Kruit et al., 2007). The canopy compensation point concentration takes into account the stomatal and soil layers. The soil compensation point concentration,  $\chi_{\text{g}}$ , in parts per billion has been calculated from the emission potential  $\Gamma_{\text{g}}$  (unitless) as a function of soil surface temperature  $T_{\text{g}}$  in kelvin according to Wentworth et al. (2014):

$$\chi_{\text{g}} = 13\,587 \times \Gamma_{\text{g}} \times e^{-(10\,396/T_{\text{g}})} \times 10^9. \quad (2)$$

A large  $\Gamma_{\text{g}}$  indicates that the soil has a high propensity to emit NH<sub>3</sub>, considering that the potential emission of NH<sub>3</sub> depends on the availability of ammonium in the soil and on the pH.  $\Gamma_{\text{g}} = [\text{NH}_4^+]/[\text{H}^+]$  concentrations were measured in the field and are available in Delon et al. (2017).

Two different models designed to simulate land–atmosphere NH<sub>3</sub> bidirectional exchange are used in this study and described below.

### 2.4.1 Inferential method (Zhang et al., 2010)

An inferential method was used to calculate the bidirectional exchange of NH<sub>3</sub>. The overall flux  $F_{\text{NH}_3}$  ( $\mu\text{g m}^{-2} \text{s}^{-1}$ ) is calculated as

$$F_{\text{NH}_3} = (\chi_{\text{cp}} - C_{\text{NH}_3}) \times V_{\text{d}}, \quad (3)$$

**Table 1.** Summary of different models used in the study, with the variables simulated and compared to measurements. All simulated and measured variables were daily averaged for the purpose of the study.

Model (resolution)	Simulated and measured variables (units)	Methods used for measured variables (resolution and reference)
Surfatm (3 h)	NH <sub>3</sub> bidirectional fluxes (ngN m <sup>-2</sup> s <sup>-1</sup> )	Closed dynamic chamber (15–20 fluxes a day, Delon et al., 2017)
	Soil surface temperature (°C)	Campbell 107 probe (15 min, Tagesson et al., 2015a)
	Sensible and latent heat fluxes (W m <sup>-2</sup> )	Eddy covariance (15 min, Tagesson et al., 2015a)
Zhang2010 (3 h)	NH <sub>3</sub> bidirectional fluxes (ngN m <sup>-2</sup> s <sup>-1</sup> )	Closed dynamic chamber (15–20 fluxes a day, Delon et al., 2017)
STEP (day)	NO biogenic fluxes (ngN m <sup>-2</sup> s <sup>-1</sup> )	Closed dynamic chamber (15–20 fluxes a day, Delon et al., 2017)
	CO <sub>2</sub> respiration fluxes (ngN m <sup>-2</sup> s <sup>-1</sup> )	Closed dynamic chamber (15–20 fluxes a day, Delon et al., 2017)
	Ammonium content (%)	Laboratory analysis (six samples per campaign, Delon et al., 2017)
	Soil temperature at two depths: 0–2 and 2–30 cm (°C)	Campbell 107 probe at two depths: 5 and 10 cm (15 min, Tagesson et al., 2015a)
	Soil moisture at two depths: 0–2 and 2–30 cm (%)	HH2 Delta probe at two depths: 5 and 10 cm (15 min, Tagesson et al., 2015a)

with  $V_d = 1/(R_a + R_b + R_c)$ , where  $V_d$  (m s<sup>-1</sup>) is the deposition velocity, determined by using the big-leaf dry deposition model of Zhang et al. (2003).  $R_a$  (s m<sup>-1</sup>) and  $R_b$  (s m<sup>-1</sup>) are the aerodynamic and quasi-laminar resistances respectively, and  $R_c$  (s m<sup>-1</sup>) is the total resistance to deposition resulting from component terms such as stomatal, mesophyll, and non-stomatal/external/cuticular and soil resistances (Flechard et al., 2013, and references therein).  $C_{\text{NH}_3}$  (µg m<sup>-3</sup>) is determined at the monthly scale from passive sampler measurements. The  $\chi_{\text{cp}}$  term (µg m<sup>-3</sup>) is calculated following the two-layer Zhang et al. (2010) model, hereafter referred to as Zhang2010. This model gives access to an extensive literature review on compensation point concentrations and emission potential values classified for 26 different land use classes (LUCs). Compensation point concentrations are calculated in the model and vary with canopy type, nitrogen content, and meteorological conditions. This model was adapted by Adon et al. (2013) for the specificity of semi-arid ecosystems such as leaf area index (LAI) or type of vegetation, assuming a ground emission potential of 400 (unitless), considered a low-end value for non-fertilized ecosystems according to Massad et al. (2010) and based on Delon et al. (2017) experimental results, and a stomatal emission potential of 100 (unitless) based on Massad et al. (2010) for grass, and on the study of Adon et al. (2013) for similar ecosystems as the one found in Dahra. Considering the bidirectional nature of NH<sub>3</sub> exchange, emission occurs if the canopy compensation point concentration is superior to the

ambient concentration (Nemitz et al., 2001). Emission fluxes are noted as positive. Meteorological forcing required for the simulation is 3 h-averaged wind speed, net radiation, pressure, relative humidity, air temperature at 2 m height, surface temperature at 5 cm depth, and rainfall. The equations used in this model are extensively described in Zhang et al. (2003, 2010), and will not be detailed here.

#### 2.4.2 The Surfatm model

The Surface-Atmosphere (Surfatm) model combines an energy budget model (following Choudhury and Monteith, 1988) and a pollutant exchange model (following Nemitz et al., 2001), which allows distinction between the soil and the plant exchange processes. As in Zhang2010, the scheme is based on the traditional resistance analogy describing the bidirectional transport of NH<sub>3</sub> governed by a set of resistances  $R_a$ ,  $R_b$ , and  $R_c$  (Hansen et al., 2017, and references therein) already described in the preceding paragraph. Surfatm includes a diffusive resistance term from the topsoil layer to the soil surface. Surfatm represents a comprehensive approach to study pollutant exchanges and their link with plant and soil functioning. The NH<sub>3</sub> exchange is directly coupled to the energy budget, which determines the leaf and surface temperatures, the humidity of the canopy, and the resistances in the layers above the soil and in the soil itself. This model has been comprehensively described in Personne et al. (2009) and more recently in Hansen et al. (2017).

The model is forced every 3 h by net radiation, deep soil temperature (30 cm), air temperature, relative humidity, wind speed, rainfall, and atmospheric  $\text{NH}_3$  concentration with monthly values from passive sampler measurements repeated every 3 h. Forcing also includes values of leaf area index (LAI, measured), canopy height  $Z_h$  (estimated), roughness length  $Z_0$  ( $0.13 Z_h$ ), displacement height  $D$  ( $0.7 Z_h$ ), stomatal emission potential (constant), ground emission potential (derived from measurements during field campaigns, constant the rest of the time), and measurement height  $Z_{\text{ref}}$  (2 m). LAI was measured according to the methodology developed in Mougin et al. (2014). Data from Dahra were measured monthly during the wet season and were not published (Mougin, personal communication). Linear interpolation was performed between these monthly estimates, and values for the dry season were found in Adon et al. (2013), for an equivalent semi-arid ecosystem in Mali, derived from MODIS (Moderate-Resolution Imaging Spectroradiometer) measurements. The ground emission potential has been set to 400 (unitless), and the stomatal emission potential has been set to 100 (unitless) as in the simulation based on Zhang2010, except during field campaign periods, where the ground emission potential was derived from experimental values (700 in J12 and J13 and 2000 in N13). In Table 2, constant input parameters are listed. Some of them were adapted to semi-arid conditions to get the best fit between measured and simulated fluxes, specified in Table 2.

The main difference between Surf atm and Zhang2010 is the presence of a SVAT (surface vegetation atmosphere transfer) model in Surf atm (Personne et al., 2009), allowing for energy budget consideration and accurate restitution of surface temperature and moisture. Simulated variables and corresponding measurements used for validation are summarized in Table 1.

## 2.5 Statistic analysis

The R software (<http://www.R-project.org>, last access: 8 May 2019) was used to provide results of simple and multiple linear regression analysis. The `cor.test()` function was used to test a single correlation coefficient  $R$ , i.e. a test for association between paired samples, using one of Pearson's product moment correlation coefficients. The  $p$  value is used to determine the significance of the correlation. If the  $p$  value is less than 0.05, the correlation is considered non-significant. The `lm()` test was used for stepwise multiple regression analysis. The adjusted  $R$  squared (i.e. normalized multiple  $R$  squared,  $R^2$ ), determines how well the model fits to the data. Again, the  $p$  value is calculated, and has to be less than 0.05 to give confidence in the significance of the determination coefficient  $R^2$ . These tests are used in the following paragraphs (i) to determine if the models are precise enough to correctly represent environmental variables like soil moisture, soil temperature, and latent and sensible heat fluxes at the annual scale and to represent measured fluxes

of  $\text{NO}$ ,  $\text{NH}_3$ , and  $\text{CO}_2$  for some periods (ii) to verify if environmental drivers, taken individually or in groups, explain the  $\text{NO}/\text{NH}_3/\text{CO}_2$  simulated fluxes and to what extent and (iii) to compare the two models used for  $\text{NH}_3$  flux modelling.

## 3 Results

### 3.1 Soil moisture, soil temperature, and land–atmosphere heat fluxes

Soil moisture simulated by STEP in the surface layer (Fig. 2a) is limited at 11 % during the wet season. This value corresponds to the field capacity calculated by STEP. The soil moisture modelling follows the tipping-bucket approach; i.e. when the field capacity is reached, the excess water is transferred to the second layer, between 2 and 30 cm. Experimental values measured at 5 and 10 cm are better represented by the model in this second layer (Fig. 2b). Linear regression gives a  $R^2$  of 0.74 (resp. 0.81), a slope of 0.98 (resp. 1.05), and an offset of 0.34 (resp. 0.32) between STEP soil moisture in the 0–2 cm (resp. 2–30 cm) layer and experimental soil moisture at 5 cm.  $R^2$  is 0.77, slope is 0.93, and offset is 0.84 between STEP soil moisture in the 2–30 cm layer and experimental soil moisture at 10 cm. The temporal dynamics given by STEP, the filling of the surface layer, and the maximum and minimum values are comparable to the data. However, the drying of the layers is sharper in the model than in measurements at the end of the wet season, leading to an underestimation of the model compared to measurements until December each year.

As a comparison, linear correlation between STEP H (STEP LE) and EC H (EC LE) gives  $R^2$  of 0.4 (0.7), for both years of simulation (Fig. 3a and b). The significant correlation between Surf atm and EC latent heat fluxes indicates that the stomatal, aerodynamic, and soil resistances are correctly characterized in the model, giving confidence in the further realistic parameterization of  $\text{NH}_3$  fluxes, despite missing values in intermediate fluxes, due to the criteria applied by the post-processing (see Supplement of Tagesson et al., 2015b).

Surf atm soil surface temperature is very close to measured soil surface temperature (Fig. 4a,  $R^2 = 0.70$ ,  $p < 0.001$  in 2012–2013). Mean annual values were 35.8 and 34.2 °C respectively for surface Surf atm and measured soil surface temperatures in 2012 and 32.4 and 33.8 °C in 2013. STEP surface temperatures (0–2 cm layer) present mean values of 32.0 °C in 2012 and 32.6 °C in 2013. Linear regression between STEP surface temperature and measured surface temperature (Fig. 4b) gives a  $R^2$  of 0.7 ( $p < 0.001$ ) for 2012–2013. Slopes and offsets are indicated in the figures.

### 3.2 Biogenic NO fluxes from soil and ammonium content

In J12, average  $\text{NO}$  fluxes are  $5.1 \pm 2.8$  and  $5.7 \pm 3.1 \text{ ngN m}^{-2} \text{ s}^{-1}$  for modelled and measured fluxes respec-



**Table 2.** Input parameters for the Surfalm model. Ranges refer to Hansen et al. (2017). All measured parameters refer to Delon et al. (2017).

Description of parameters in Surfalm	Value in this study (range)	Sources
Time step	3 h	
Characteristic length of leaves	0.03 m (0.03–0.5)	Minimum value
Total soil depth	0.92 m	
Soil density	1500 kg m <sup>−3</sup>	
Radiation attenuation coefficient in the canopy	0.7 (0.5–0.8)	Estimated
Wind attenuation coefficient in the canopy	2.3 (1.5–5)	Estimated
Initial soil moisture	0.09 kg(H <sub>2</sub> O) kg(soil) <sup>−1</sup>	Measured
Dry soil moisture	0.02 kg(H <sub>2</sub> O) kg(soil) <sup>−1</sup>	Measured
Field capacity	0.14 kg(H <sub>2</sub> O) kg(soil) <sup>−1</sup>	Measured
Wilting point	0.02 kg(H <sub>2</sub> O) kg(soil) <sup>−1</sup>	Measured
Thermal conductivity of wet soil layers	2.5 W m <sup>−1</sup> K <sup>−1</sup> (1.6–2.2)	Estimated
Thermal conductivity of dry soil layers	1.5 W m <sup>−1</sup> K <sup>−1</sup> (0.2–0.3)	Estimated
Depth of temperature measurements	0.3 m	Measured
Soil porosity	0.45 (0.25–0.4)	Estimated specifically for semi-arid ecosystems
Soil tortuosity	2.5 (2–4)	Estimated specifically for semi-arid ecosystems

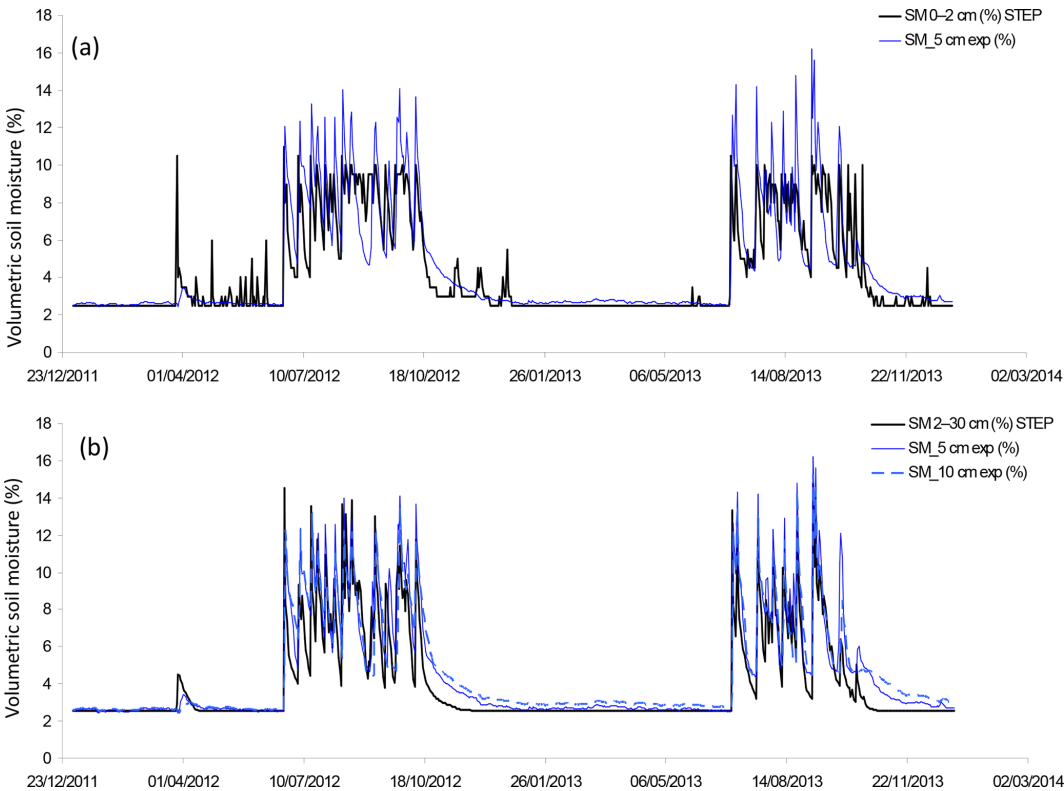


**Figure 2.** (a) Volumetric soil moisture simulated by STEP in the first layer (0–2 cm) in black and soil moisture measured at 5 cm in blue, as a percentage, at a daily scale. (b) Volumetric soil moisture simulated by STEP in the second layer (2–30 cm) in black, soil moisture measured at 5 cm as a blue solid line, measured at 10 cm as a blue dotted line, as a percentage, at a daily scale.

tively. In J13, average NO fluxes are  $10.3 \pm 3.3$  and  $5.1 \pm 2.1 \text{ ngN m}^{-2} \text{ s}^{-1}$  for modelled and measured fluxes respectively. In N13, average NO fluxes are  $2.2 \pm 0.3$  and  $4.0 \pm 2.2 \text{ ngN m}^{-2} \text{ s}^{-1}$  for modelled and measured fluxes respectively. Emission fluxes are noted as positive.

In Fig. 5, the model represents the daily fluxes for 2012 and 2013 and is compared to measurements. The model is comprised within the standard deviation of the measurements in J12 and N13 but overestimates fluxes in J13. Figure 6 reports nine points of measured ammonium from Delon et

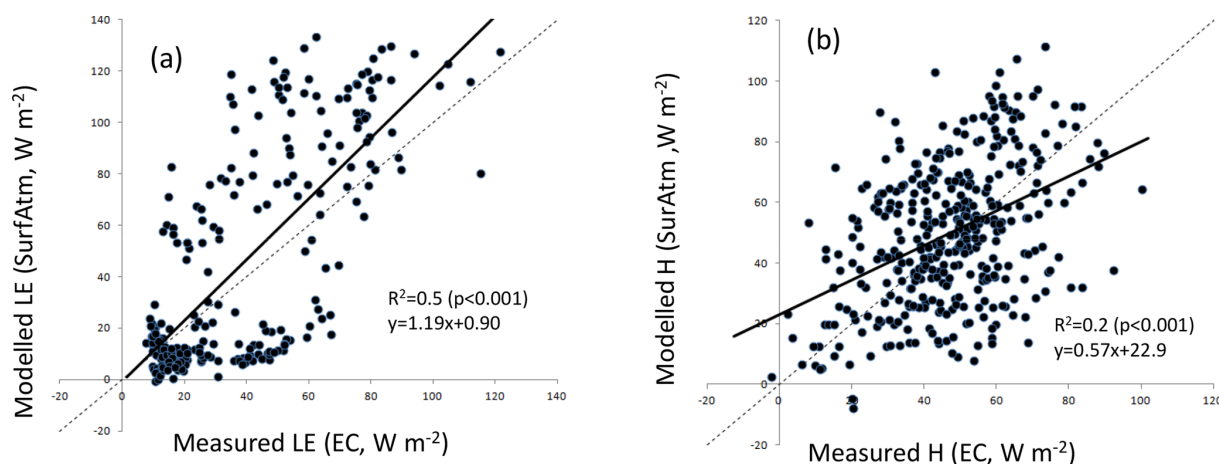


**Figure 3.** (a) Daily modelled latent heat flux in SurfAtm vs. daily measured latent heat flux, in watts per square metre; (b) daily modelled sensible heat flux in SurfAtm vs. daily measured sensible heat flux, in watts per square metre. The thick black line is for the linear regression, and the dashed black line is the 1 : 1 line. Available measured EC data are more numerous for H than for LE due to the criteria applied by the post-processing (see Supplement of Tagesson et al., 2015b).

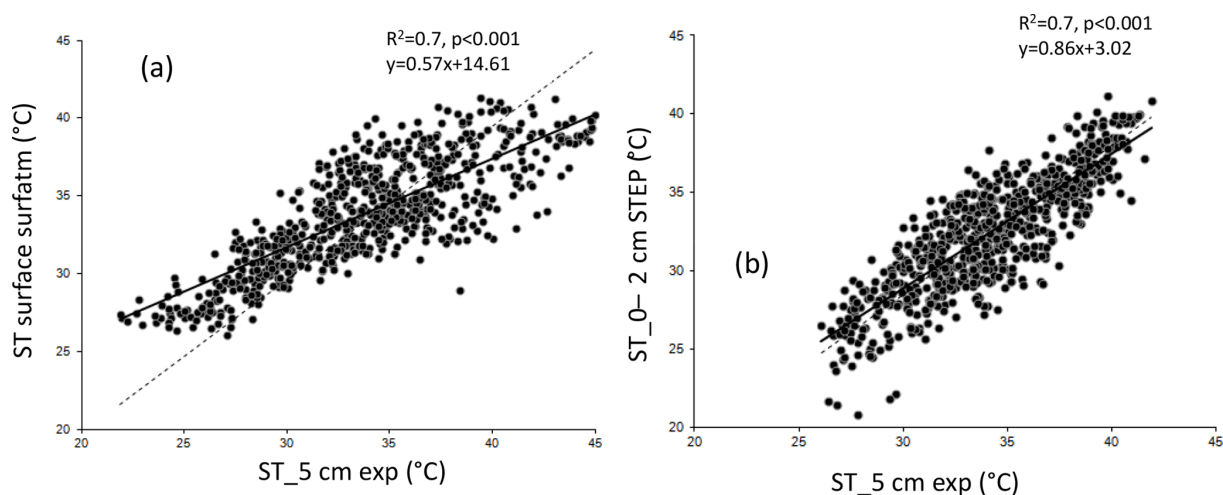


**Figure 4.** (a) Modelled daily surface temperature in SurfAtm vs. measured daily temperature at 5 cm depth; (b) modelled daily surface temperature in STEP (0–2 cm layer) vs. measured daily temperature at 5 cm depth. The thick black line is for the linear regression, and the dashed black line is the 1 : 1 line.

al. (2017), showing an overestimation of released N during the J13 wet season and an underestimation at the end of the wet season (as N13).

Modelled dry and wet season NO fluxes are respectively  $2.5 \pm 2.5$  and  $6.2 \pm 4.1 \text{ ngN m}^{-2} \text{ s}^{-1}$  for both 2012 and 2013, and the simulation gives a mean flux of  $3.6 \pm 2.9 \text{ ngN m}^{-2} \text{ s}^{-1}$  for the entire study period. Wet season fluxes represent 51 % of the annual mean, even though it only lasts 3 to 4 months. Simulated NO fluxes are significantly correlated with measured soil moisture at 5 cm depth ( $R^2 = 0.42$ ,  $p < 0.001$ , slope = 0.65, offset = 0.69) and 10 cm depth ( $R^2 = 0.43$ ,  $p < 0.001$ , slope = 0.72, offset = 0.33) for both years, but not directly with soil temperature. A multiple linear regression model involving soil moisture at 5 cm

depth, soil temperature at 5 and 30 cm depth, and wind speed to explain simulated NO fluxes leads to a  $R^2$  of 0.43 ( $p < 0.001$ ). These parameters have been shown as important drivers of NO emissions in several previous studies, such as Homyak et al. (2016), Medinets et al. (2015), or Delon et al. (2007). Indeed, as detailed in Appendix B, NO fluxes in STEP–GENDEC–NOflux are calculated by an equation derived from an artificial neural network (ANN) algorithm, trained with data from temperate and tropical ecosystems, taking into account these four parameters, together with sand percentage, soil pH, and N input.

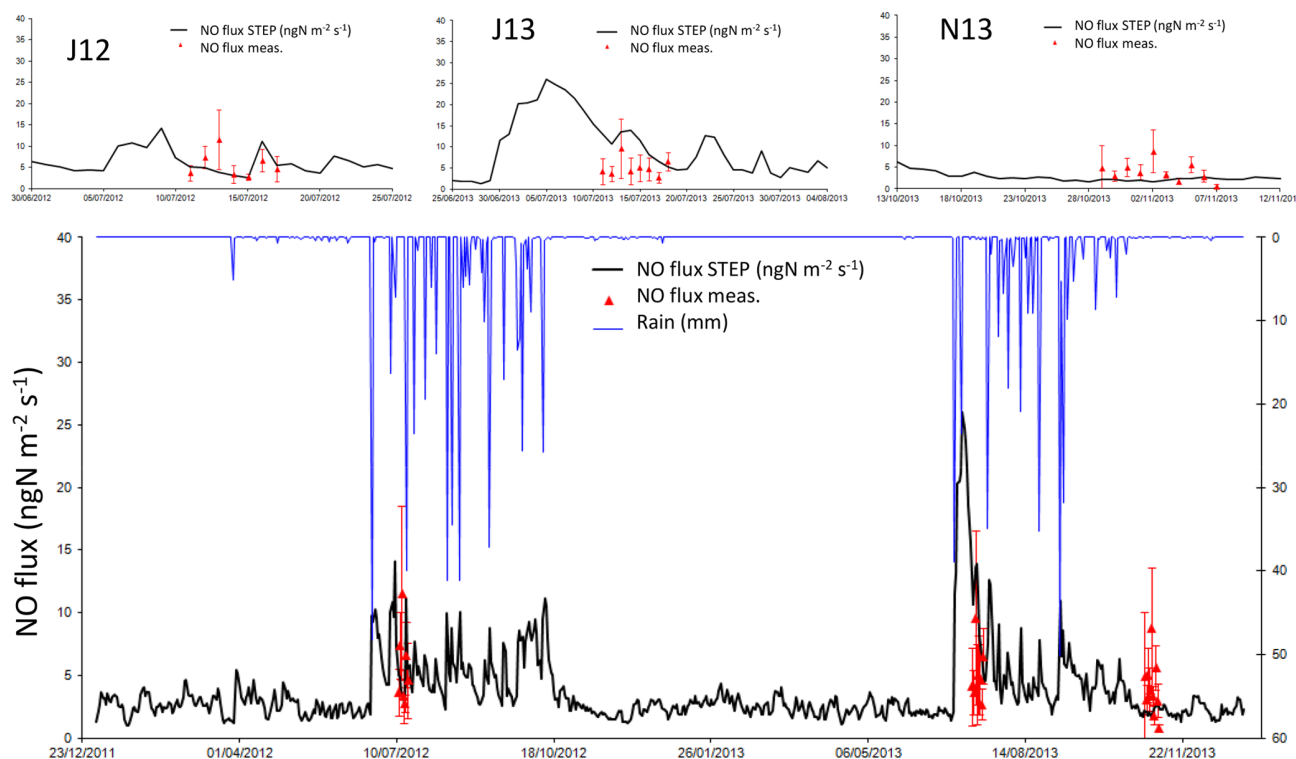


**Figure 5.** Daily NO flux simulated by STEP–GENDEC–NOFlux ( $\text{ngN m}^{-2} \text{s}^{-1}$ , black line) and daily averaged NO flux measurements during the three field campaigns (red triangles). Error bars in red give the standard deviation for measurements at the daily scale. Rain is represented by the blue line in millimetres in the bottom panel. The upper panels show a focus on each field campaign.

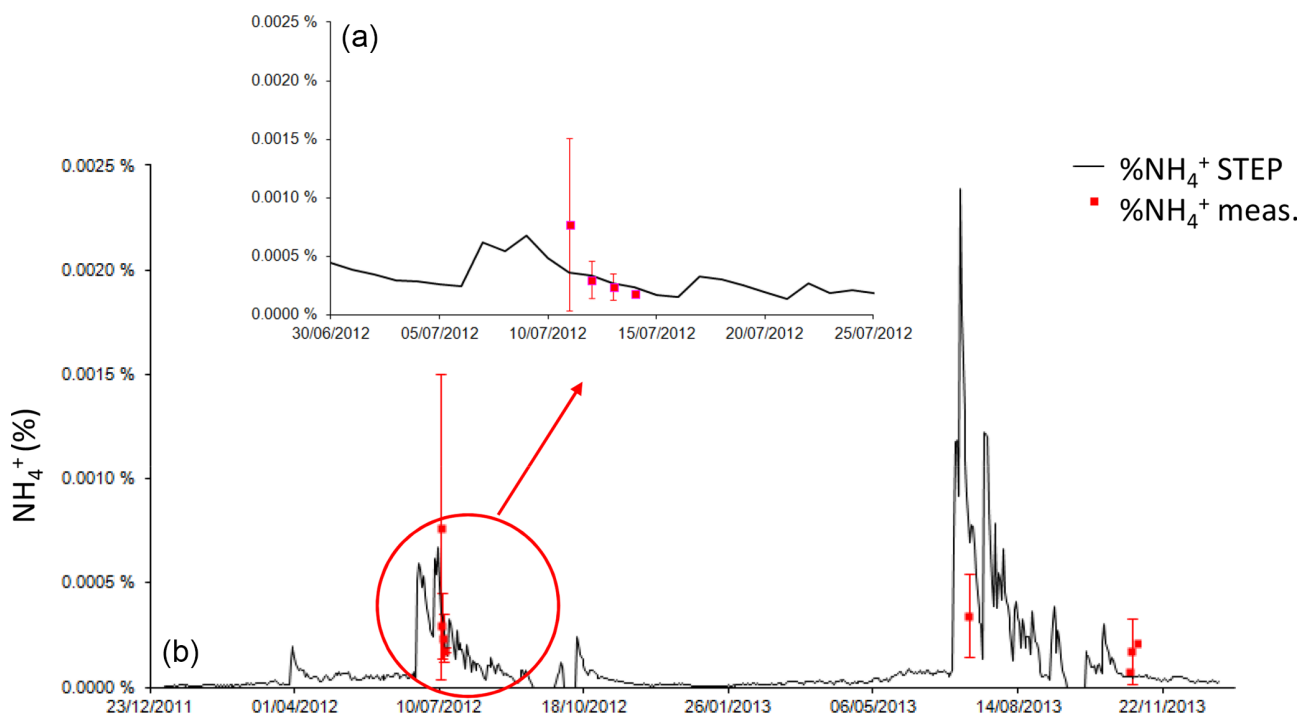


**Figure 6.** Daily ammonium simulated by STEP–GENDEC (% , black line) and daily averaged ammonium measurement (red squares) during the field campaigns. Error bars in red give the standard deviation at the daily scale for measurements. The upper panel is a focus of J12.

### 3.3 Soil CO<sub>2</sub> respiration

Soil respiration includes soil heterotrophic respiration, which refers to the decomposition of dead soil organic matter (SOM) by soil microbes, and root respiration, including all respiratory processes occurring in the rhizosphere (Xu et al., 2016). The simulated respiration of aboveground biomass is not included as in measured data.

In J13, the average measured flux is  $2.6 \pm 0.6 \text{ gC m}^{-2} \text{ d}^{-1}$ , and the average modelled flux is  $1.9 \pm 0.4 \text{ gC m}^{-2} \text{ d}^{-1}$ . The correlation between the two data sets is not significant. In N13, the average measured flux is  $0.78 \pm 0.11 \text{ gC m}^{-2} \text{ d}^{-1}$ , and the average modelled flux is  $0.18 \pm 0.02 \text{ gC m}^{-2} \text{ d}^{-1}$ . The two data sets are not correlated. November fluxes are less important than July fluxes, as illustrated by both the model and the measurements (Fig. 7), and as previously shown with eddy covariance data (Tagesson et al., 2015a). Simulated respiration fluxes are in the range of measured fluxes in J13, but appear to underestimate measured fluxes in N13 (Fig. 7). The simulated autotrophic respiration (roots + aboveground biomass) is shown, together with the heterotrophic (microbes) respiration, to check for a possible role of aboveground biomass in comparison with measurements (Fig. 8). As expected, the heterotrophic respiration is higher than the autotrophic respiration before and after the growth of the vegetation, i.e. at the beginning and end of the wet season in 2012, or during precipitation dry spells (e.g. in J13). At the end of the wet season, the late peaks of simulated heterotrophic respiration are linked to late rain events because autotrophic respiration is no more effective when vegetation is not growing anymore. Adding the autotrophic respiration to the heterotrophic respiration does not help to better fit the measured respiration in N13.

Average dry and wet season simulated soil respiration are respectively  $0.3 \pm 0.7$  and  $1.0 \pm 0.4 \text{ gC m}^{-2} \text{ d}^{-1}$ , while the annual mean is  $0.5 \pm 0.7 \text{ gC m}^{-2} \text{ d}^{-1}$ . This annual mean is below global estimates for grassland ( $2.2 \text{ gC m}^{-2} \text{ d}^{-1}$ ) and deserts partially vegetated ( $1.0 \text{ gC m}^{-2} \text{ d}^{-1}$ ; Xu et al., 2016). The wet season has the largest contribution (57 %) to the annual respiration budget (with wet seasons of 114 and 81 d in 2012 and 2013 respectively).

Simulated daily respiration from microbes and roots is significantly correlated with measured soil moisture at 5 cm depth with  $R^2 = 0.50$ ,  $p < 0.001$ , slope = 0.17, offset = 0.26 and 10 cm depth with  $R^2 = 0.5$ ,  $p < 0.001$ , slope = 0.19, offset = −0.37 for both years, whereas soil field-measured respiration shows a lower correlation with surface soil moisture, with  $R^2 = 0.4$ ,  $p = 0.09$ , slope = 0.03, offset = −0.07 in J13 and  $R^2 = 0.3$ ,  $p = 0.1$ , slope = 0.02, offset = −0.02 in N13.

### 3.4 NH<sub>3</sub> bidirectional exchange

NH<sub>3</sub> fluxes were simulated by two different models: Surf atm (Personne et al., 2009) and Zhang2010 (Fig. 9). The same ambient concentrations deduced from in situ measurements

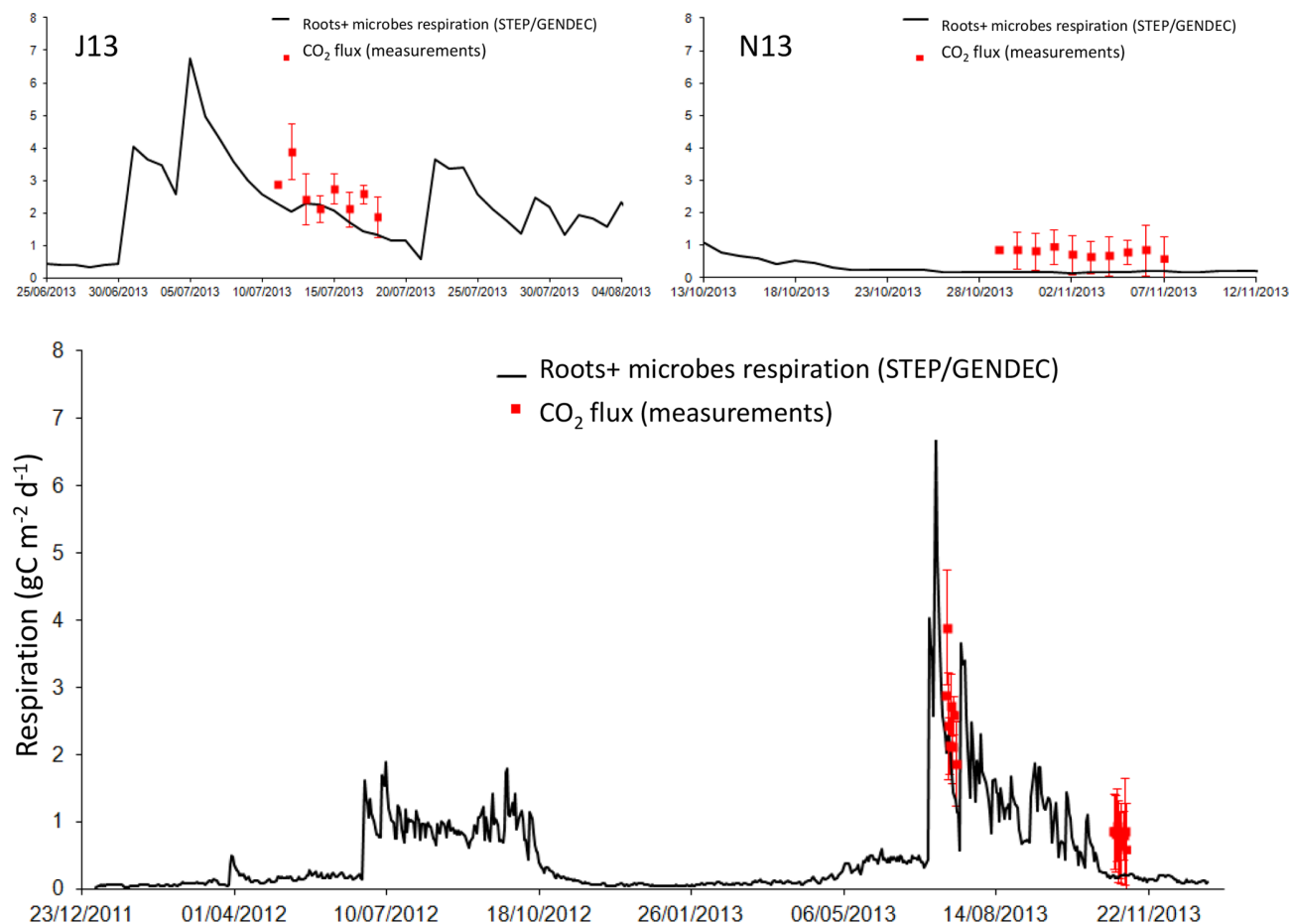
are prescribed in both models. Average fluxes are reported in Table 2. In J12, simulated fluxes are not significantly correlated with measured data. In J13, Surf atm and measurement fluxes are not significantly correlated ( $R^2 = 0.2$ ,  $p = 0.2$ ). In N13, Surf atm and measured fluxes are not significantly correlated ( $R^2 = 0.2$ ,  $p = 0.2$ ), and Zhang2010 and measured fluxes are significantly correlated ( $R^2 = 0.5$ ,  $p = 0.01$ , slope = 1.5, offset = −3.8).

Figure 9 shows alternative changes between low NH<sub>3</sub> emission and low deposition. This switch occurs during the dry seasons (from mid-October to the end of June). Indeed, monthly averaged compensation point and ambient concentration values are quite similar during the dry seasons. Compensation point concentration averaged during the 2012 and 2013 dry seasons is  $3.8 \pm 1.5$  ppb, and averaged ambient concentration is  $4.3 \pm 1.5$  ppb for the same period. If the 2012 and 2013 dry seasons are considered separately, the values of the means remain the same. Low deposition dominates when air humidity is sufficiently high, roughly above 25 % (before and after the wet season), whereas low emission dominates when air humidity is low (< 25 %).

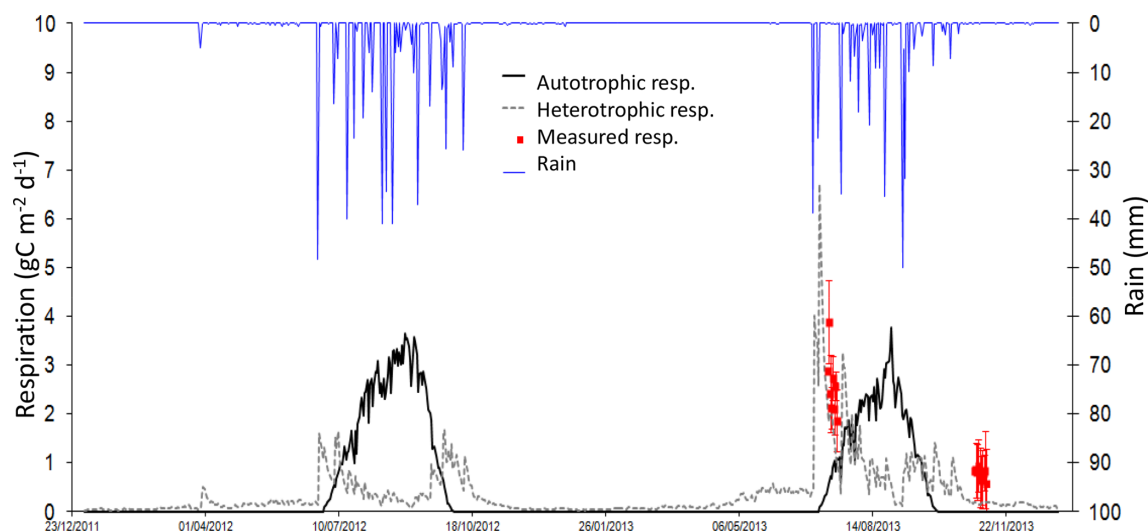
The net dry and wet season fluxes reported in Table 3 are in a similar range as NH<sub>3</sub> fluxes calculated by Adon et al. (2013) using Zhang2010 at comparable Sahelian sites in Mali and Niger. NH<sub>3</sub> fluxes ranged between −3.2 and  $0.9 \text{ ngN m}^{-2} \text{ s}^{-1}$  during the dry season and between −14.6 and  $-6.0 \text{ ngN m}^{-2} \text{ s}^{-1}$  during the wet season.

Figure 10 shows the partition between the different contributions of soil and vegetation to the NH<sub>3</sub> fluxes in Surf atm and Zhang2010. During the wet season, the contributions of vegetation and soil in Surf atm (Zhang2010) are  $-6.3 \pm 3.7$  ( $-0.8 \pm 0.36 \text{ ngN m}^{-2} \text{ s}^{-1}$ ) and  $2.0 \pm 1.9 \text{ ngN m}^{-2} \text{ s}^{-1}$  ( $-7.3 \pm 3.0 \text{ ngN m}^{-2} \text{ s}^{-1}$ ) respectively for both years. During the dry season, vegetation (i.e. stomata + cuticles) and soil contributions are low:  $-0.9 \pm 1.7$  and  $0.7 \pm 0.6 \text{ ngN m}^{-2} \text{ s}^{-1}$  respectively in Surf atm and  $-0.4 \pm 0.5$  and  $-0.5 \pm 2.3 \text{ ngN m}^{-2} \text{ s}^{-1}$  in Zhang2010, as reported in Table 4. In N13, at the end of the wet season, the soil contribution is  $2.9 \pm 0.7 \text{ ngN m}^{-2} \text{ s}^{-1}$  in Surf atm, whereas it is  $-2.6 \pm 0.8 \text{ ngN m}^{-2} \text{ s}^{-1}$  in Zhang2010.

In Fig. 10a, the total net flux above the canopy in Surf atm results from an emission flux from the soil and a deposition flux onto the vegetation via stomata and cuticles, especially during the wet season. Conversely, the total flux in Zhang2010 in Fig. 10b results from a strong deposition flux on the soil and a very low deposition flux onto the vegetation. This is explained by a strong contribution of deposition on cuticles in Surf atm (Fig. 10c) whereas it is close to zero in Zhang2010 (Fig. 10d). In Surf atm, emission from stomata also occurs but it is largely offset by the deposition on leaf surfaces, which leads to a deposition flux onto vegetation (Sutton et al., 1995). In Surf atm, the deposition on cuticles is effective until the end of the wet season, whereas deposition through stomata lasts until the vegetation is completely dry, i.e. approximately 2 months after the end of the wet season.



**Figure 7.** Daily root and microbe respiration in milligrammes of carbon per square metre per day simulated by STEP–GENDEC (black line), and daily averaged soil respiration measurements (red squares) during two field campaigns. Error bars in red give the standard deviation at the daily scale. The upper panels show a focus of J13 and N13 field campaigns.



**Figure 8.** Daily autotrophic (roots + green vegetation, black line) and daily heterotrophic (microbes, grey dashed line) respiration ( $\text{mgC m}^{-2} \text{d}^{-1}$ ) and rain (blue line, mm). Averaged daily measurements of soil respiration as red squares, with standard deviation.

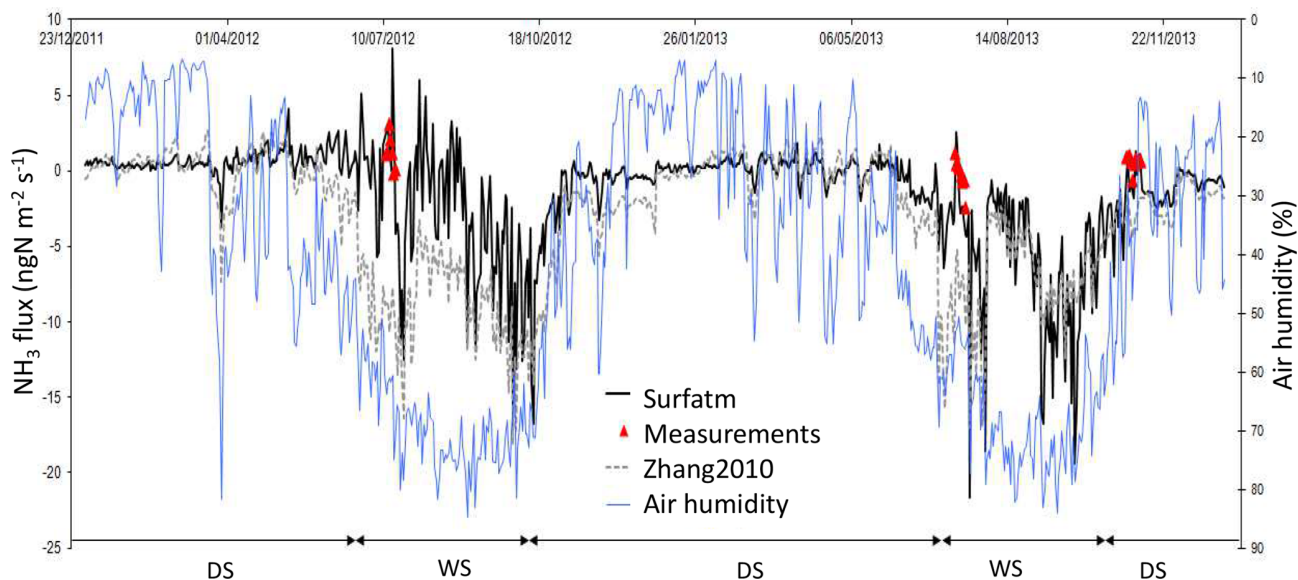


**Figure 9.** Daily  $\text{NH}_3$  flux ( $\text{ngN m}^{-2} \text{s}^{-1}$ ) simulated by Surf atm (black line) and Zhang2010 (grey dashed line) and daily averaged  $\text{NH}_3$  flux measurements during three field campaigns (red triangles). Error bars in red stand for standard deviation at the daily scale. Air humidity as a percentage (blue line). DS: dry season; WS: wet season.

**Table 3.** Averaged  $\text{NH}_3$  fluxes for measurements and the Surf atm and Zhang2010 models during specific periods. Measurements are available during the three field campaigns and not at the annual or seasonal scale.

Period/ $\text{NH}_3$ fluxes	Measurements ( $\text{ngN m}^{-2} \text{s}^{-1}$ )	Surf atm ( $\text{ngN m}^{-2} \text{s}^{-1}$ )	Zhang2010 ( $\text{ngN m}^{-2} \text{s}^{-1}$ )
J12	$1.3 \pm 1.1$	$2.6 \pm 2.6$	$-9.0 \pm 0.9$
J13	$-0.1 \pm 1.1$	$-1.7 \pm 2.4$	$-7.8 \pm 2.2$
N13	$0.7 \pm 0.5$	$-0.2 \pm 1.1$	$-2.8 \pm 0.9$
2012		$-0.9 \pm 3.3$	$-3.5 \pm 4.6$
		$(-0.3 \pm 1.0 \text{ kgN ha}^{-1} \text{ yr}^{-1})$	$(-0.3 \pm 1.0 \text{ kgN ha}^{-1} \text{ yr}^{-1})$
2013		$-2.0 \pm 3.7$	$-2.7 \pm 3.8$
		$(-0.6 \pm 0.3 \text{ kgN ha}^{-1} \text{ yr}^{-1})$	$(-0.8 \pm 1.2 \text{ kgN ha}^{-1} \text{ yr}^{-1})$
Dry season		$-0.2 \pm 1.6$	$-0.9 \pm 2.3$
Wet season		$-4.3 \pm 4.8$	$-8.1 \pm 3.2$

On the basis of the different averages for each contributing flux in Table 4, we estimate that the soil is a net source of  $\text{NH}_3$  during the wet season, while the vegetation is a net sink in Surf atm, and the soil is a net sink in Zhang2010.

#### 4 Discussion

##### 4.1 $\text{NH}_3$ exchanges

###### 4.1.1 Relevance of monthly $\text{NH}_3$ concentration input vs. daily $\text{NH}_3$ flux outputs

In the two models,  $C_{\text{NH}_3}$  used as input data arises from passive sampler measurements, integrated at the monthly scale (see Sect. 2.2.2). Output fluxes are provided at a 3 h timescale, averaged at the daily scale for the purpose of this

study. The relevance of using monthly  $\text{NH}_3$  concentrations instead of concentrations with finer resolution in time has already been approached in the literature. Riddick et al. (2014, 2016) have used ALPHA samplers to measure  $\text{NH}_3$  concentrations at the scale of the week and/or the month. They have noticed that time-averaged  $\text{NH}_3$  fluxes from these samplers provided estimated fluxes similar to those calculated from online sampling. In the case of passive sampling concentration measurements, meteorological and area sources of uncertainty can still be accounted for in the flux calculation. Riddick et al. (2014) conclude that active and passive sampling strategies give similar results, which support the use of low-cost passive sampling measurements at remote locations where it is often logistically hard to deploy expensive active sampling methods for flux measurements. These statements have been confirmed in Loubet et al. (2018), and provide a



**Table 4.** Contributions of vegetation and soil to the total  $\text{NH}_3$  flux in Surf atm and Zhang2010, wet season mean, dry season mean, and annual mean, for both years of simulation.

Average flux and standard deviation	$F_{\text{total}}$ (net flux) ( $\text{ngN m}^{-2} \text{s}^{-1}$ )	$F_{\text{soil}}$ ( $\text{ngN m}^{-2} \text{s}^{-1}$ )	$F_{\text{vegetation}}$ ( $= F_{\text{stom}} + F_{\text{cut}}$ ) ( $\text{ngN m}^{-2} \text{s}^{-1}$ )	$F_{\text{stom}}$ ( $\text{ngN m}^{-2} \text{s}^{-1}$ )	$F_{\text{cut}}$ ( $\text{ngN m}^{-2} \text{s}^{-1}$ )
Dry seasons Surf atm	$-0.2 \pm 1.6$	$0.7 \pm 0.6$	$-0.9 \pm 1.7$	$-0.4 \pm 0.8$	$-0.5 \pm 1.2$
Wet seasons Surf atm	$-4.3 \pm 4.8$	$2.0 \pm 1.9$	$-6.3 \pm 3.7$	$-1.5 \pm 2.2$	$-4.8 \pm 2.7$
2012–2013 Surf atm	$-1.4 \pm 3.5$	$1.1 \pm 1.3$	$-2.5 \pm 3.5$	$-0.7 \pm 1.5$	$-1.8 \pm 2.7$
Dry seasons Zhang2010	$-0.9 \pm 2.3$	$-0.5 \pm 2.3$	$-0.4 \pm 0.5$	$-0.02 \pm 0.01$	$-0.4 \pm 0.5$
Wet seasons Zhang2010	$-8.1 \pm 3.2$	$-7.3 \pm 3.0$	$-0.8 \pm 0.3$	$-0.03 \pm 0.01$	$-0.7 \pm 0.3$
2012–2013 Zhang2010	$-3.1 \pm 4.2$	$-2.6 \pm 4.0$	$-0.5 \pm 0.4$	$-0.02 \pm 0.01$	$-0.5 \pm 0.4$

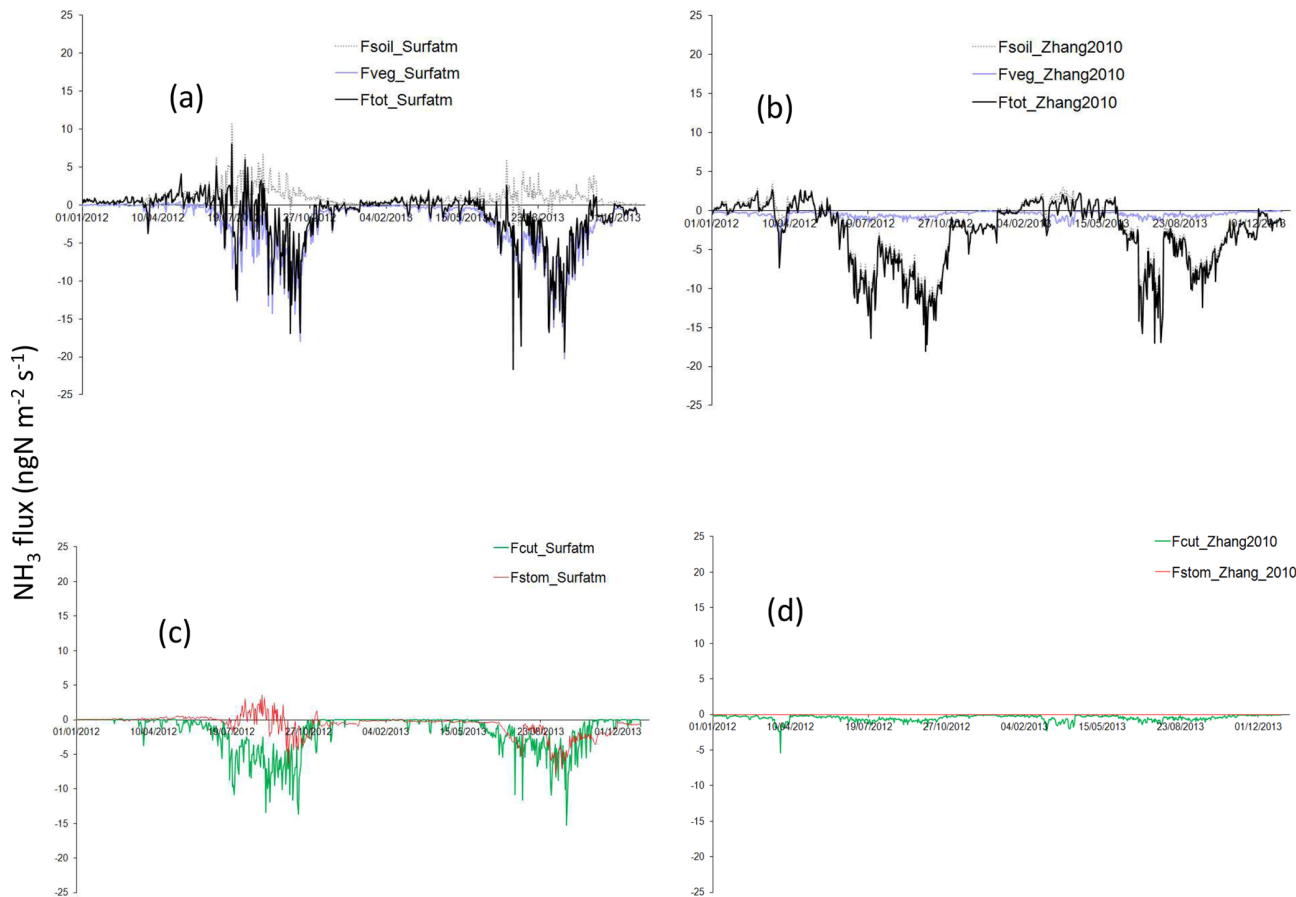


**Figure 10.** Daily  $\text{NH}_3$  flux ( $\text{ngN m}^{-2} \text{s}^{-1}$ ) partitioned between soil and vegetation. The black line is for total net flux ( $F_{\text{tot}}$ ), the grey dashed line is for soil flux ( $F_{\text{soil}}$ ), and the blue line is for vegetation flux ( $F_{\text{veg}}$ ) for Surf atm in (a) and for Zhang2010 in (b). The red line is for stomatal flux ( $F_{\text{stom}}$ ) and the green line is for cuticular flux ( $F_{\text{cut}}$ ) for Surf atm in (c) and for Zhang2010 in (d).

valuable reason to use monthly concentrations as inputs in the present study.

#### 4.1.2 $\text{NH}_3$ deposition flux variation

Dahra is a grazed savanna where the main source of  $\text{NH}_3$  emission to the atmosphere is the volatilization of livestock excreta (Delon et al., 2012); the excreta quantity and qual-

ity is at a maximum at the end of the wet season, (Hiernaux et al., 1998; Hiernaux and Turner, 2002; Schlecht and Hiernaux, 2004) because animals are better fed. In August, a strong leaching of the atmosphere occurs, which decreases the  $\text{NH}_3$  atmospheric concentration (not shown here), compared to July concentration, and the deposition flux decreases as well. Indeed, if the concentration decreases from July to

August whereas the canopy compensation point remains stable, the flux will decrease as shown by Eq. (3).

August is the month with the maximum ammonium wet deposition, which leads to a strong leaching of the atmosphere and explains the decrease in the  $\text{NH}_3$  concentration (Laouali et al., 2012).

#### 4.1.3 Role of soil moisture and soil temperature in $\text{NH}_3$ fluxes

A significant correlation is found between Zhang2010 fluxes and measured soil moisture at 5 cm depth ( $R^2 = 0.6$ ,  $p < 0.01$ , slope =  $-1.2$ , offset =  $2.1$ ) for 2012–2013. Surf atm fluxes and measured soil moisture at 5 cm depth are also significantly correlated with  $R^2 = 0.3$ ,  $p < 0.01$ , slope =  $-0.7$ , offset =  $1.7$  for 2012–2013, and this correlation is higher if only the dry season is considered ( $0.7$  and  $0.5$  respectively). A weak but significant correlation is found between Surf atm fluxes and soil surface temperature ( $R^2 = 0.2$ ,  $p < 0.001$ , slope =  $0.14$ , offset =  $33.9$ ) for both wet seasons, whereas it is not found with Zhang2010 fluxes. An explanation may be that the  $\text{NH}_3$  exchange in Surf atm is directly coupled with the energy balance via the surface temperature (Personne et al., 2009). A stepwise multiple linear regression analysis was performed between Zhang2010 fluxes and  $\text{NH}_3$  ambient concentrations, air humidity, wind speed, and soil surface temperature and moisture, for both years of simulation. The model selection was performed by adding each variable step by step, i.e. the best combination was chosen with the best associated significant  $R^2$  ( $p < 0.05$ ). The resulting model gives a  $R^2$  of  $0.9$  ( $p < 0.001$ ), showing a large interdependence of the above-cited parameters on  $\text{NH}_3$  fluxes, whereas the correlation between  $\text{NH}_3$  fluxes and each individual parameter is not significant. While the isolated soil temperature effect is not demonstrated, these complex interactions between influencing parameters suggest that the contribution of soil temperature to  $\text{NH}_3$  fluxes, together with other environmental parameters, becomes relevant.

As for Zhang2010 fluxes, a stepwise multiple linear regression analysis is run between Surf atm  $\text{NH}_3$  fluxes and  $\text{NH}_3$  concentrations, air humidity, wind speed, soil surface temperature, and latent heat fluxes.  $R^2$  is  $0.6$  with  $p < 0.001$ . The nested influences of environmental parameters in Surf atm are highlighted. These interactions become more complex with the energy balance effect, but may be more accurate in representing the partition between surface and plant contributions.

#### 4.1.4 Contribution of soil and vegetation to the net $\text{NH}_3$ flux

In Surf atm, during the wet season, deposition on the vegetation through stomata and cuticles dominates the exchange. Indeed, during rain events, the cuticular resistance becomes small and cuticular deposition dominates despite an increase

in soil emission. This increase is due to an increase in the deposition velocity of  $\text{NH}_3$ , after the humidity response of the surface, and a decrease in the canopy compensation point, sensitive to the surface wetness (Wichink-Kruit et al., 2007). In Zhang2010, despite the difference in magnitude, cuticular deposition increases as well during the wet season, but is dominated by deposition on the soil.

During the dry season, aboveground herbaceous dry biomass stands for a few months after the end of the wet season when the soil becomes bare, and the vegetation effect is negligible in both models. At the end of wet season 2013, the soil contribution to the total flux increases significantly in Surf atm due to the increase in the ground emission potential prescribed at 2000 (instead of 400 for the rest of the year, to be consistent with measurements noted in Delon et al., 2017).

#### 4.1.5 Surf atm versus Zhang2010 $\text{NH}_3$ bidirectional models

The two models are based on the same two-layer model approach developed in Nemitz et al. (2001). In the two models, the ground emission potential and the  $\text{NH}_3$  ambient concentrations are prescribed. The comparison of modelled and measured flux values in Fig. 9 shows differences, especially for results predicted by Zhang2010. This is partly because in Surf atm the ground emission potential varies with time and was specifically modified for the field campaign periods, whereas this parameter does not vary in Zhang2010. The lack of variability of the ground emission potential in Zhang2010 highlights the sensitivity of fluxes to this specific parameter for 1-D modelling in semi-arid soils. The abrupt transitions between seasons need a certain flexibility of the ground emission potential to represent the changes in flux direction.

In Surf atm, the temperatures (above and in the soil) are calculated through the sensible heat flux; the humidity and evaporation at the soil surface are calculated through the latent heat flux. The resistances needed for the compensation point concentration and for the flux calculation are deduced from the energy budget. This allows us to simultaneously take into account the role of temperature and humidity of the soil. In Zhang2010, the  $R_a$ ,  $R_b$ , and  $R_c$  resistances are calculated directly from the meteorological forcing, and the soil resistance is prescribed. Again, the flexibility of this parameter is more adapted than fixed values for 1-D modelling, and this may lead to completely different repartitions of the fluxes between the soil and the vegetation, as shown in Fig. 10. This difference in flux repartition highlights the importance of the choice in the type of soil and/or vegetation for the simulations.

However, the close correlation between both models ( $R^2 = 0.5$ ,  $p < 0.01$ , slope =  $0.6$ , offset =  $0.4$ ) indicates a similar representation of the net flux in each model and emphasizes clear changes at the transition between seasons.



## 4.2 Effect of soil moisture, soil temperature, and soil characteristics on exchange processes

For most of the biomes the temperature strongly governs soil respiration through metabolism of plants and microbes (Lloyd and Taylor, 1994; Reichstein et al., 2005; Tagesson and Lindroth, 2007). However, in our results we found no significant correlation between soil surface temperature and trace gas fluxes. This confirms that in the semi-arid tropical savannas, physiological activity is not limited by temperature (Archibald et al., 2009; Hanan et al., 1998, 2011; Tagesson et al., 2016a, 2015a). Instead, soil moisture variability overrides temperature effects as also underlined by Jia et al. (2006). Indeed, for low soil moisture conditions, slight changes in soil moisture may have a primordial effect, while temperature effect on microbial activities is not observable (Liu et al., 2009). This may explain why soil temperature and NO, CO<sub>2</sub>, and NH<sub>3</sub> fluxes are not correlated at the annual scale (dominated by dry months) as mentioned in the preceding paragraphs. Due to higher soil moisture in wet seasons ( $8.1 \pm 2.7\%$  vs.  $3.2 \pm 1.5\%$  in dry seasons), soil temperature effect becomes visible, elevated temperatures may increase microbial activity, and changes in soil temperature may have an influence on N turnover and N exchanges with the atmosphere (Bai et al., 2013).

The over- or underestimations of NO emissions in the model in Fig. 5 may be explained by the ammonium content shown in Fig. 6. Released N is overestimated during the J13 wet season and underestimated at the end of the wet season (as N13), when the presence of standing straw may lead to N emissions in addition to soil emissions, not accounted for in the model because litter is not yet buried. The slight underestimation of modelled soil moisture (Fig. 2) at the end of the wet season may also explain why modelled fluxes of NO (Fig. 5) and CO<sub>2</sub> (Fig. 7) are lower than measured fluxes. Furthermore, the model over-predicts the death rate of microbes and subsequently underestimates the CO<sub>2</sub> respired, whereas microbes and residues of root respiration persist in the field despite low soil moisture. The large spatial heterogeneity in measurements may be explained by variations in soil pH and texture and by the presence of livestock and the short-term history of the Dahra site, i.e. how livestock have trampled, grazed, and deposited manure during the different seasons and at different places. This spatial variation is evidently not represented in the 1-D model, where unique soil pH and soil texture are given, as well as a unique input of organic fertilization by livestock excreta.

During the dry season, substrates become less available for microorganisms, and their diffusion is affected by low-soil-moisture conditions (Xu et al., 2016). The microbial activity slows down gradually and stays low during the dry season (Wang et al., 2015; Borken and Matzner, 2009). De Bruin et al. (1989) have experimentally shown that drying did not kill the microbial biomass during alternating wet–dry conditions at a Sahelian site. It is therefore likely that the transition from

activity to dormancy or death at the end of the wet season is too abrupt in the STEP–GENDEC–NOFlux model, leading to smaller NO and CO<sub>2</sub> fluxes than the still rather large measured fluxes. Furthermore, the two first layers of the soil in the model dry up more sharply than what measurements indicate, and the lower modelled soil moisture has an effect on modelled fluxes.

During the wet season, and just before and after, the link between soil or leaf wetness related to air humidity and NH<sub>3</sub> dry deposition is straightforward, as NH<sub>3</sub> is highly soluble in water. Water droplets, and thin water films formed by deliquescent particles on leaf surfaces increase NH<sub>3</sub> dry deposition (Flechard and Fowler, 1998). This process is easily reproduced by the two models used in this study, as shown in Fig. 9 where a net NH<sub>3</sub> dry deposition flux is observed during the wet season.

With wet season NO fluxes being more than 2 times higher than dry season fluxes, results emphasize the influence of pulse emissions in that season. This increase at the onset of the wet season over the Sahel, due to the drastic change in soil moisture, has been previously highlighted by satellite measurements of the N<sub>2</sub>O column, by Vinken et al. (2014), Hudman et al. (2012), Jaegle et al. (2004), and Zörner et al. (2016). After the pulses of NO at the beginning of the wet season (Fig. 5), emissions decrease most likely because the available soil mineral N is used by plants during the growing phase of roots and green biomass, especially in 2013, and is less available for the production of NO to be released to the atmosphere (Homyak et al., 2014; Meixner and Fenn, 2004; Krul et al., 1982). During the wet season, NO emissions to the atmosphere in the model are reduced by 18 % due to plant uptake (compared to NO emissions when plant uptake is not taken into account). Indeed, N uptake by plants is enhanced when transpiration increases during the wet season (Appendix C).

## 4.3 Coupled processes of NO, CO<sub>2</sub>, and NH<sub>3</sub> emissions

Larger CO<sub>2</sub> and NO fluxes were seen at the beginning of the wet season (Figs. 5 and 7), compared to the core of the wet season and to the dry season. This can be explained by the rapid response of the soil decomposers to the increase in soil moisture leading to a rapid decomposition of the litter buried during the preceding dry season and a rapid increase in ammonium as shown in Fig. 6. A pool of enzymes remains in the soil during the dry season and ensures decomposition with the first rains even when microorganism population is not yet fully developed. Austin et al. (2004) have stated that as microbial substrates decompose rapidly, microbes will be sufficiently supplied for growth and respiration, involving CO<sub>2</sub> emissions, and the excess N will therefore be mineralized. Indeed, the NH<sub>4</sub><sup>+</sup> dynamics control nitrification and volatilization processes (Schlesinger and Peterjohn, 1991; McCalley et al., 2011). The NH<sub>4</sub><sup>+</sup> pool may be depleted via nitrification, involving NO emissions, and in parallel volatilized, in-

volving concomitant  $\text{NH}_3$  emissions. Conversely, a major depletion of the  $\text{NH}_4^+$  pool via nitrification may favour deposition of  $\text{NH}_3$  if  $\text{NH}_4^+$  is no longer available in the soil to be volatilized.

During the dry season, as the microbial activity is reduced to its lower limit, the N retention mechanism in microbial biomass does not work anymore, N retention is linked to the mineralization of organic C caused by heterotrophic microbial activity and allows N to be available for plants, and mineral N may accumulate in the soil during this time (Perroni-Ventura et al., 2010; Austin et al., 2004). Therefore, N loss should neither occur via  $\text{NH}_3$  volatilization during that period, nor via NO emission. Furthermore, the very low soil moisture and air humidity do not stimulate  $\text{NH}_3$  deposition on bare soil or vegetation, if present, during the dry season, knowing that  $\text{NH}_3$  is very sensitive to ambient humidity.  $\text{NH}_3$ , NO, and  $\text{CO}_2$  fluxes are affected by the same biotic and abiotic factors, including amount of soil organic C, N quantity and availability, soil oxygen content, soil texture, soil pH, soil microbial communities, hydro-meteorological conditions, amount of above- and below-ground biomass, species composition, and land use (Xu et al., 2016; Pilegaard et al., 2013; Chen et al., 2013).

At the end of the wet season, the increase in the senescent aboveground biomass increases the quantity of litter, which leads to an input of new organic matter to the soil and therefore a new pool of mineral N available for the production of NO and  $\text{NH}_3$  to be released to the atmosphere, at a time when herbaceous species would no longer benefit from it. This process has been highlighted in Delon et al. (2015) in a similar dry savanna in Mali. Furthermore, NO and  $\text{NH}_3$  emissions are suspected to come from the litter itself, as shown in temperate forests by Gritsch et al. (2016), where NO litter emissions increase with increasing moisture.

In the STEP–GENDEC–NOFlux model respiration and soil NO fluxes were significantly correlated ( $R^2 = 0.6$ ,  $p < 0.001$ , slope = 0.2, offset =  $-0.2$ ), but not directly in the measurements, due to the spatial variability of the site. The microbial activity is not efficient enough in the model when the soil moisture is low, whereas in measurements, as for NO fluxes, this microbial activity seems to remain at a residual level leading to a release of both NO and  $\text{CO}_2$  to the atmosphere (Delon et al., 2017). A lagged relationship may somehow be displayed in measurements if measured NO fluxes are shifted by 1 d (i.e.  $\text{CO}_2$  is in advance) in J13, then  $R^2 = 0.6$ ,  $p = 0.03$ , slope = 62.4, and offset =  $-2.5$  ( $R^2 = 0.2$  if not shifted), highlighting a lag between  $\text{CO}_2$  and NO emission processes. If the same lag is applied in model predictions, then  $R^2 = 0.6$ ,  $p < 0.001$ , slope = 3.3, and offset = 2.0, showing that soil respiration and nitrification processes (causing NO release) are closely linked by microbial processes through soil microorganisms that trigger soil respiration and decomposition of soil organic matter (Xu et al., 2008; Ford et al., 2007). This 1 d lag however has to be considered an open question. The exact lag duration should be

studied more thoroughly, but highlights the close relationship between processes of nitrification and respiration anyway.

## 5 Conclusions

This study has shown that  $\text{NH}_3$ , NO, and  $\text{CO}_2$  exchanges between the soil and the atmosphere are driven by the same microbial processes in the soil, presupposing that moisture is sufficient to engage them, and taking into account the very specific climatic conditions of the Sahel region. Indeed, low soil and air water content are a limiting factor in semi-arid regions in N cycling between the surface and the atmosphere, whereas processes of N exchange rates are enhanced when water content of the exchange zone, where microbial processes occur, becomes more important. The role of soil moisture involved in N and C cycles is remarkable and obvious in initiating microbial and physiological processes. Conversely, the role of soil temperature is not as obvious because its amplitude of variation is weak compared to soil moisture. Temperature effects are strongly alleviated when soil moisture is low in the dry season, and become again an influencing parameter in the wet season for N exchange.  $\text{CO}_2$  respiration fluxes in this study are not influenced by soil temperature variations, overridden by soil moisture variation at the seasonal and annual scale.  $\text{NH}_3$  bidirectional fluxes, simulated by two different models, have shown a high sensitivity to the ground emission potential. The possibility of adjusting this parameter to field measurements has greatly improved the capacity of the Surfalm model to fit the observation results.

The understanding of underlying mechanisms, coupling biogeochemical, ecological, and physico-chemical process approaches, are very important for an improved knowledge of C and N cycling in semi-arid regions. The contrasted ecosystem conditions due to drastic changes in water availability have important non-linear impacts on the biogeochemical N cycle and ecosystem respiration. This affects atmospheric chemistry and climate, indicating a strong role of coupled surface processes within the Earth system. If changes in precipitation regimes occur due to climate change, the reduction of precipitation regimes may affect regions not considered as semi-arid until now and drive them to semi-arid climates involving exchange processes such as those described in this study. Additionally, an increase in demographic pressure leading to increases in livestock density and changes in land uses will cause changes in soil physical and chemical properties, vegetation type, and management, important factors affecting N and C exchanges between natural terrestrial ecosystems and the atmosphere.

*Code availability.* The Surfalm model is available from Erwan Personne (erwan.personne@agroparistech.fr) on request. STEP–GENDEC–NOflux is available from Eric Mougin (eric.mougin@

get.omp.eu) on request. Zhang2010 is available from Leiming Zhang (leiming.zhang@ec.gc.ca) on request.

*Data availability.* Data used in this study are not publicly available. They are available upon request from Claire Delon (claire.delon@aero.obs-mip.fr) for modelling outputs and measurements and in Delon et al. (2017) for measurements. Data from the meteorological station in Dahra are available from Torbern Tagesson (torbern.tagesson@ign.ku.dk) and Rasmus Fensholt (rf@geo.ku.dk) upon request.

## Appendix A: Details on STEP formulations

**Table A1.** Daily climatic data of the Dahra station used for the forcing of the STEP–GENDEC–NOFlux model.

Variable	Symbol	Unit	Source
Rainfall	$P$	mm	Dahra meteorological station
Maximum air temperature, minimum air temperature	$T_{\text{a,max}}, T_{\text{a,min}}$	°C	Dahra meteorological station
Incident global radiation	$R_{\text{glo}}$	MJ m <sup>−2</sup>	Dahra meteorological station
Mean relative air humidity	Hr	%	Dahra meteorological station
Wind speed	ws	m s <sup>−1</sup>	Dahra meteorological station

**Table A2.** Site parameters necessary for initialization of the STEP–GENDEC–NOFlux model.

Parameter	Symbol	Unit	Value	Source
Latitude	lat	°	15°24′10″ N,	GPS measurement
Longitude	long	°	15°25′56″ W	GPS measurement
Soil depth	Sd	m	3	Measurement
Number of soil layers	$N_i$	–	4	
Thickness of layer $i$	$e_i$	cm	2/28/70/200	
Sand content of layer $i$	Sand <sub><math>i</math></sub>	%	89/89/91/91	Delon et al. (2017)
Clay content of layer $i$	Clay <sub><math>i</math></sub>	%	7.9/7.9/7.4/5; 5	Delon et al. (2017)
pH value of layer $i$	pH <sub><math>i</math></sub>	–	6.4/6.4/6.4/6.4	Delon et al. (2017)
Initial water content of layer $i$	Shum <sub><math>i</math></sub>	mm	0.4/8/10/38	Field measurement
Initial soil temperature of layer $i$	Ts <sub><math>i</math></sub>	°C	23.5/23.9/28/30	Field measurement
Run-off(on) coefficient	C <sub>Ruiss</sub>	–	0	Endorheic site
Soil albedo	$\omega_s$	–	0.45	Station scale, satellite
Initial dry mass	BM <sub>s0</sub>	g m <sup>−2</sup>	10	Delon et al. (2015)
Initial litter mass	BM <sub>l0</sub>	g m <sup>−2</sup>	30	Delon et al. (2015)
C <sub>3</sub> / C <sub>4</sub> herb proportion	C <sub>3</sub> C <sub>4</sub>	%	43/67	Field measurement
Dicotyledon. contribution	Dicot	%	43	Field measurement
Root mass proportion of layer $i$ (layers 2 to 4)	Root	%	75/20/5	Mougin et al. (1995)
Initial soil carbon content	Cs	gC m <sup>−2</sup>	50	Unpublished data
Initial soil N content	Ns	gN m <sup>−2</sup>	3	Unpublished data

**Table A3.** Model parameters used to run the STEP–GENDEC–NOFlux model.

Parameter	Symbol	Unit	Value [range]	Source
Vegetation albedo	$\omega_v$	–	0.2	Station measurement, satellite
Canopy extinction coefficient for green vegetation	$k_c$	–	0.475	Mougin et al. (2014)
PAR extinction coefficient	$k_{fAPAR}$	–	0.581	Mougin et al. (2014)
Maximum conversion efficiency	$\varepsilon_{max}$	$\text{gDM MJ}^{-1}$	4 [4–8]	Scaling parameter
Initial aboveground green mass	$BM_{g0}$	$\text{g m}^{-2}$	0.8 [0.1, 3]	Scaling parameter
Specific plant area at emergence	$SLA_{g0}$	$\text{m}^2 \text{g}^{-1}$	0.018 [0.01–0.03]	Scaling parameter
Slope of the relation $SLA(t)$	$k_{SLA}$	–	0.028	Unpublished data (Mougin)
Specific plant area for dry mass	$SLA_d$	$\text{m}^2 \text{g}^{-1}$	0.0144	Unpublished data (Mougin)
Shoot maintenance respiration cost	$m_{cs}$	(–)	0.015	Breman and de Ridder (1991)
Root maintenance respiration cost	$m_{cr}$	(–)	0.01	Breman and de Ridder (1991)
Shoot growth conversion efficiency	$Y_G$	(–)	0.75	McCree (1970)
Root growth conversion efficiency	$Y_{Gr}$	(–)	0.8	Bachelet et al. (1989)
Green mass senescence rate	$s$	$\text{d}^{-1}$	0.00191	Mougin et al. (1995)
Live root senescence rate	$s_r$	$\text{d}^{-1}$	0.00072	Nouvellon (2000)
Optimal temperature for photosynthesis	$T_{max}$	$^{\circ}\text{C}$	38	Penning de Vries and Djitéye (1982)
Leaf water potential for 50 % stomatal closure	$\psi_{1/2}$	MPa	0.6	Rambal and Cornet (1982)
Shape parameter	$n$	(–)	5	Rambal and Cornet (1982)
Minimum stomatal resistance	$r_{s,min}$	$\text{d m}^{-1}$	100	Körner et al. (1979)
Parameters of the canopy height curve	$a, b, c$	(–)	–0.0000024, 0.0055, 0.047	Mougin et al. (1995)
Infiltration time constant	$K_i$	$\text{cm d}^{-1}$	1200/120/120/80	Casenave and Valentin (1989)
Parameters of the soil water resistance equation	$a_s, b_s$	(–)	4140, 805	Camillo and Gurney (1986)
Parameters of the soil characteristic retention curve	$a_i, b_i$	(–)	3.95/5.42/6.97/9.80 2.93/2.71/2.59/2.43	Modified from Cornet (1981)
Field capacity	$FC_i$	$\text{m}^3 \text{m}^{-3}$	0.093/0.093/0.086/0.081	Prescribed
Psychrometric constant	$\gamma$	$\text{Bar } ^{\circ}\text{C}^{-1}$	0.00066	Monteith (1995)
Allocation factor	$a_{factor}$	(–)	0.5 [0,1]	Mougin et al. (1995)

**Table A4.** Equations, variables, parameters, and constants used in STEP. Variables are in *italics*. DM: dry matter.

Equations	Parameters, variables, constants	Unit	Source
Soil Temperature			
$T_{\text{smax}} = T_{\text{amax}} + (Er + 0.35T_{\text{amax}}) \times Eb$ $T_{\text{smin}} = T_{\text{amin}} + 0.006 \text{ BMg} - 1.82$ $Er = 24.07(1 - \exp(-0.000038 R_{\text{glo}}))$ $Eb = \exp(-0.0048 \text{ BMg}) - 0.13$	$T_{\text{smax(min)}}$ : max(min) soil temperature $T_{\text{amax(min)}}$ : max(min) air temperature $R_{\text{glo}}$ : global radiation BMg: above-ground green mass	$^{\circ}\text{C}$ $^{\circ}\text{C}$ $\text{kJ m}^{-2}$ $\text{gDM m}^{-2}$	Parton et al. (1984)
Carbon budget			
$Vcft = 1 - \exp(-k_c \text{LAI})$	Vcft: total vegetation cover fraction LAI: leaf area index $k_c$ : canopy extinction coefficient for green vegetation (Table A3)	$\text{m}^2 \text{ m}^{-2}$ $\text{m}^2 \text{ m}^{-2}$ (-)	Mougin et al. (2014)
$Vcfg = Vcft(\text{LAIg} / \text{LAI})$ $Vcfd = Vcft(\text{LAId} / \text{LAI})$ $\text{LAIg} = \text{SLAg} \times \text{BMg}$ $\text{LAId} = \text{SLAd} \times \text{BMd}$ $\text{LAI} = \text{LAIg} + \text{LAId}$	Vcfg: green vegetation cover fraction Vcfd: dry vegetation cover fraction LAIg: green LAI LAId: dry LAI LAI: total LAI Bmd: above-ground dry mass	$\text{m}^2 \text{ m}^{-2}$ $\text{m}^2 \text{ m}^{-2}$ $\text{m}^2 \text{ m}^{-2}$ $\text{m}^2 \text{ m}^{-2}$ $\text{m}^2 \text{ m}^{-2}$ $\text{m}^2 \text{ m}^{-2}$	Mougin et al. (2014) Mougin et al. (1995)
$\text{SLAg} = \text{SLAg}_0 \exp(-k_{\text{SLA}} t)$	SLAg: specific green leaf area SLAd: specific plant area for dry mass (Table A3) $k_{\text{SLA}}$ : constant slope (Table A3) SLAg <sub>0</sub> : scaling parameter (Table A3) $t$ : time	$\text{m}^{-2} \text{ kg}^{-1}$ $\text{m}^{-2} \text{ kg}^{-1}$ (-) $\text{m}^2 \text{ kg}^{-1}$ s	Mougin et al. (1995)
Water budget			
if $P < 5I = P$ ; if $P > 5I = P + C_{\text{Ruiss}} (2P - 10)$	$P$ : precipitation $I$ : infiltration $C_{\text{Ruiss}}$ : run-off coefficient	$\text{mm d}^{-1}$ $\text{mm d}^{-1}$ (-)	Hiernaux (1984)
$dW_1 / dt = I - E_1 - D_1$	1: first soil layer, $i = 2$ to 4 $W_i$ : water content in layer $i$	$\text{mm d}^{-1}$ $\text{mm d}^{-1}$	Manabe (1969)
$dW_i / dt = D_{i-1} - E_i - \text{Tr}_i - D_i$	$E_i$ : evaporation in layer $i$ $D_i$ : drainage in layer $i$ $\text{Tr}_i$ : transpiration in layer $i$	$\text{mm d}^{-1}$ $\text{mm d}^{-1}$ $\text{mm d}^{-1}$	
if $W_i > \text{FCD}_i = (D_{i-1} - \text{FC}_i) / \text{Ak}_i$ with $\text{Ak}_i = e_i / K_i$	$\text{FC}_i$ : field capacity in layer $i$ (Table 3) $\text{Ak}_i$ : time constant $e_i$ : layer depth (Table A3) $K_i$ : infiltration time constant (Table A3)	$\text{mm d}^{-1}$ $\text{d}^{-1}$ cm $\text{cm d}^{-1}$	
$\Psi_{s,i} = a_i W_i^{-b_i}$	$\Psi_{s,i}$ : soil water potential in layer $i$ $W_i$ : water content in layer $i$ $a_i$ : retention curve parameter $b_i$ : retention curve parameter	MPa	
$W_{s,i} = 0.332 - 7.251 \times 10^{-4} (\text{Sand}_i) + 0.1276 \log_{10}(\text{Clay}_i)$	$W_{s,i}$ : soil water content at saturation in layer $i$ $\text{Sand}_i$ : sand content of layer $i$ (Table A2) $\text{Clay}_i$ : clay content of layer $i$ (Table A2)	$\text{m}^3 \text{ m}^{-3}$ % %	Saxton et al. (1986)

Table A4. Continued.

Equations	Parameters, variables, constants	Unit	Source
Soil Temperature			
$E = Vcfd(sA + \rho CpD / r_{as}) / \lambda(s + \gamma(1 + r_{ss}/r_{as}))$ $Tr = Vcfg(sA + \rho CpD / r_{ac}) / (\lambda(s + \gamma(1 + r_{sc}/r_{ac})))$ $s = 4098e_s / (237 + Ta)^2$ $r_{ss} = a_s (W_{sat} - W_1) - b_s$ $W_{sat} = 0.332 - 7.251 \times 10^{-4} Sand_1 + 0.1276 \log(Clay_1)$	$E$ : evaporation $Tr$ : transpiration $D$ : water vapour deficit, deduced from $e_s$ $s$ : saturating vapour slope $A$ : available energy (Rn–G) $Cp$ : specific heat air capacity (Table A3) $r_{as}$ : soil aerodynamic resistance $r_{ss}$ : soil surface resistance $r_{ac}$ : aerodynamic resistance $\lambda$ : vaporization latent heat $\gamma$ : psychrometric constant (Table A3) $\rho$ : volumic air mass $a_s$ : parameter (Table A3) $b_s$ : parameter (Table A3) $W_{sat}$ : soil water content at saturation $W_1$ : soil water content of layer 1	$mm\ d^{-1}$ $mm\ d^{-1}$ $Bar$ $Bar$ $Bar\ K^{-1}$ $MJ\ d^{-1}$ $MJ\ kg^{-1}\ C^{-1}$ $d\ m^{-1}$ $d\ m^{-1}$ $d\ m^{-1}$ $MJ\ m^{-3}$ $bar\ C^{-1}$ $kg\ m^{-3}$ $(-)$ $(-)$ $mm\ d^{-1}$ $mm\ d^{-1}$	Monteith (1965) Camillo and Gurney (1986)
$r_{sc} = r_{s\ min} (1 + (\psi/\psi_{1/2})^n)$	$r_{sc}$ : canopy stomatal resistance $r_{s\ min}$ : minimum stomatal resistance $\psi_{1/2}$ : leaf water potential for 50 % stomatal closure $\psi$ : leaf water potential $n$ : shape factor (Table 3)	$d\ m^{-1}$ $d\ m^{-1}$ $MPa$ $MPa$ $(-)$	Rambal and Cornet (1982)
$h_c = aBMg^2 + bBMg + c$	$h_c$ : canopy height $a, b, c$ : parameters (Table A3)	m	Mougin et al. (1995)
Growth model (shoots and roots)			
$dBMg / dt = \alpha_1 a_{factor} PSN + \alpha_2 BMg$ $dBMr / dt = \alpha_3 (1 - a_{factor}) PSN + \alpha_4 BMr$ $\alpha_1 = 0.75(1 - e^{-ag}) / ag, \alpha_2 = e^{-ag},$ $\alpha_3 = 0.8(1 - e^{-ad}) / ad, \alpha_4 = e^{-ad}$ $ag = 0.01125 \times 2^{(Ta/10-2)}$ $ad = 0.0008 \times 2^{(Ts1/10-2)}$ $PSN = 0.466 R_{glo} \times \varepsilon_i \times f(\Psi)$ $\times f(T) \varepsilon_{max}$ $BMr / BMg = 1.2 / (2 + 0.01 BMg)$ $f(T) = 1 - 0.0389(T_{max} - T_a)$ $f(\Psi) = r_{s\ min} / r_{sc}$ $\varepsilon_i = 0.187 \log(1 + 9.808 LAI_g)$	$a_{factor}$ : allocation factor $BMr$ : root mass $PSN$ : photosynthesis $\varepsilon_{max}$ : maximum conversion efficiency (Table A3) $T_{max}$ : optimal temperature for photosynthesis (Table A3) $T_a$ : air temperature $T_{s1}$ : soil temperature layer 1	$(-)$ $g\ DM\ m^{-2}$ $g\ DM\ m^{-2}$ $g\ DM\ MJ^{-1}$ $^{\circ}C$ $^{\circ}C$ $^{\circ}C$	Mougin et al. (1995)
Respiration (shoots and roots)			
$R_m = m_s YG\ BMg$ $m_s = m_{cs} (2.0^{**}(T_s/10 - 2))$	$R_m$ : shoot respiration $m_s$ : shoot maintenance $m_{cs}$ : shoot maintenance respiration cost (Table A3) $YG$ : shoot growth conversion efficiency (Table A3) $T_s$ : soil surface temperature	$g\ DM\ m^{-2}$ $(-)$ $(-)$ $(-)$ $^{\circ}C$	McCree (1970)
$R_g = (1 - YG)aPSN$	$R_g$ : shoot growth	$g\ DM\ m^{-2}$	Thornley and Cannell (2000)

Table A4. Continued.

Equations	Parameters, variables, constants	Unit	Source
Soil Temperature			
$R_{mr} = m_r YGr BMr$ $m_r = m_{cr} (2.0^{Ts/10 - 2})$	$R_{mr}$ : root respiration $YGr$ : root growth conversion efficiency (Table A3) $m_r$ : root maintenance $m_{cr}$ : root maintenance respiration cost (Table A3)	$g DM m^{-2}$ (–) (–) (–)	
$R_{gr} = (1 - YGr)[(1 - a)PSN]$	$R_{gr}$ : root growth	$g DM m^{-2}$	
Senescence			
$BMd = s BMg$ $BMrd = s_r BMr$	$s$ : green mass senescence rate (Table A3) $s_r$ : dry mass senescence rate (Table A3) $BMrd$ : dry root mass	$d^{-1}$ $d^{-1}$ $g DM m^{-2}$	



## Appendix B: Equations used in NOflux for NO flux calculation from ANN parameterization

$$\text{NOflux} = c_{15} + c_{16} \times \text{NOfluxnorm} \text{ kg N ha}^{-1} \text{ d}^{-1},$$

$$\text{NOfluxnorm} = w_{24} + w_{25} \tanh(S1) + w_{26} \tanh(S2) + w_{27} \tanh(S3),$$

where NOfluxnorm is the normalized NO flux.

$$S1 = w_0 + \sum_{i=1}^7 w_i x_{j,\text{norm}},$$

$$S2 = w_8 + \sum_{i=9}^{15} w_i x_{j,\text{norm}},$$

$$S3 = w_{16} + \sum_{i=17}^{23} w_i x_{j,\text{norm}},$$

where  $j$  is 1 to 7, and  $x_{1,\text{norm}}$  to  $x_{7,\text{norm}}$  correspond to the seven normalized inputs, as follows:

$$j = 1 : x_{1,\text{norm}} = c_1 + c_2 \times (\text{surface soil temperature}),$$

$$j = 2 : x_{2,\text{norm}} = c_3 + c_4 \times (\text{surface WFPS}),$$

$$j = 3 : x_{3,\text{norm}} = c_5 + c_6 \times (\text{deep soil temperature}),$$

$$j = 4 : x_{4,\text{norm}} = c_7 + c_8 \times (\text{fertilization rate}),$$

$$j = 5 : x_{5,\text{norm}} = c_9 + c_{10} \times (\text{sand percentage}),$$

$$j = 6 : x_{6,\text{norm}} = c_{11} + c_{12} \times \text{pH},$$

$$j = 7 : x_{7,\text{norm}} = c_{13} + c_{14} \times (\text{wind speed}).$$

Soil surface temperature is in degrees Celsius, surface WFPS as a percentage, deep soil temperature in degrees Celsius, fertilization rate in kilogrammes of nitrogen per hectare per day, sand percentage as a percentage, pH unitless, and wind speed in metres per second.

Weights  $w$  and normalization coefficients  $c$  are given in Table B1.

**Table B1.** Weights and coefficients for ANN calculation of NO flux.

$w_0$	0.561	$w_{14}$	1.611	$c_1$	−2.454
$w_1$	−0.439	$w_{15}$	0.134	$c_2$	0.143
$w_2$	−0.435	$w_{16}$	−0.213	$c_3$	−4.609
$w_3$	0.501	$w_{17}$	0.901	$c_4$	0.116
$w_4$	−0.785	$w_{18}$	−5.188	$c_5$	−2.717
$w_5$	−0.283	$w_{19}$	1.231	$c_6$	0.163
$w_6$	0.132	$w_{20}$	−2.624	$c_7$	−0.364
$w_7$	−0.008	$w_{21}$	−0.278	$c_8$	5.577
$w_8$	−1.621	$w_{22}$	0.413	$c_9$	−1.535
$w_9$	0.638	$w_{23}$	−0.560	$c_{10}$	0.055
$w_{10}$	3.885	$w_{24}$	0.599	$c_{11}$	−25.55
$w_{11}$	−0.943	$w_{25}$	−1.239	$c_{12}$	3.158
$w_{12}$	−0.862	$w_{26}$	−1.413	$c_{13}$	−1.183
$w_{13}$	−2.680	$w_{27}$	−1.206	$c_{14}$	0.614
				$c_{15}$	3.403
				$c_{16}$	9.205

### Appendix C: Nitrogen uptake by plants

In STEP the seasonal dynamics of the herbaceous layer are a major component of the Sahelian vegetation, and are represented through the simulation of the following processes: water fluxes in the soil, evaporation from bare soil, transpiration of the vegetation, photosynthesis, respiration, senescence, litter production, and litter decomposition at the soil surface. Faecal matter deposition and decomposition are also included from the livestock total load given as an input parameter.

The N uptake by plants (absorption of mineral N by plant roots) is calculated by the product of the soil water absorption by roots, with the mineral N concentration in the soil water. In the STEP model, daily root absorption is equal to the daily transpiration, which depends on climatic conditions (global radiation, air temperature, wind velocity, and air relative humidity), soil water potential (water content in soil layers), and hydric potential of the plant, which controls its stomatal aperture (and then the transpiration). Transpiration is calculated with the Penman–Monteith equation (Monteith, 1965), in which the stomatal resistance depends on the plant hydric potential, itself depending on the soil moisture and climatic conditions. For equivalent climatic conditions, a dry soil involves a high potential, a closure of stomata, and a reduction of the transpiration. Conversely, a humid soil involves a low potential, open stomata, and large transpiration. The plant hydric potential is calculated daily with transpiration equivalent to root absorption, which itself is calculated from the difference between soil and plant potentials (Mougin et al., 1995).

**Author contributions.** CD, CGL, and DS planned and designed the research. EP and BL developed the Surf atm model, EM, CD, and VLD developed the STEP–GENDEC–NOflux model, MA provided model results with the Zhang2010 model, and RF and TT provided data from the Dahra meteorological station. All authors participated in the writing of the paper.

**Competing interests.** The authors declare that they have no conflict of interest.

**Acknowledgements.** This study was financed by the French CNRS-INSU (Centre National de la Recherche Scientifique – institute National des Sciences de l’Univers), through the LEFE –CHAT comity (Les Enveloppes Fluides et l’Environnement – Chimie Atmosphérique). The authors thank the IRD (Institut de Recherche et de développement) local support for logistical help in Senegal, and the Centre de Recherches Zootechniques (CRZ) de Dahra of the Institut Sénégalais de Recherches Agricoles (ISRA) for their logistical help during the field campaigns. TT was funded by SNSB (Dnr95/16).

**Review statement.** This paper was edited by Jens-Arne Subke and reviewed by two anonymous referees.

## References

- Adon, M., Galy-Lacaux, C., Yoboué, V., Delon, C., Lacaux, J.P., Castera, P., Gardrat, E., Pienaar, J., Al Ourabi, H., Laouali, D., Diop, B., Sigha-Nkamdjou, L., Akpo, A., Tathy, J. P., Lavenu, F., and Mougin E.: Long term measurements of sulfur dioxide, nitrogen dioxide, ammonia, nitric acid and ozone in Africa using passive samplers, *Atmos. Chem. Phys.*, 10, 7467–7487, <https://doi.org/10.5194/acp-10-7467-2010>, 2010.
- Adon, M., Galy-Lacaux, C., Delon, C., Yoboue, V., Solmon, F., and Kaptue Tchuente, A. T.: Dry deposition of nitrogen compounds ( $\text{N}_2\text{O}$ ,  $\text{HNO}_3$ ,  $\text{NH}_3$ ), sulfur dioxide and ozone in west and central African ecosystems using the inferential method, *Atmos. Chem. Phys.*, 13, 11351–11374, <https://doi.org/10.5194/acp-13-11351-2013>, 2013.
- Archibald, S. A., Kirton, A., van der Merwe, M. R., Scholes, R. J., Williams, C. A., and Hanan, N.: Drivers of inter-annual variability in Net Ecosystem Exchange in a semi-arid savanna ecosystem, South Africa, *Biogeosciences*, 6, 251–266, <https://doi.org/10.5194/bg-6-251-2009>, 2009.
- Assouma, M. H., Serça, D., Guerin, F., Blanfort, V., Lecomte, P., Traoré, I., Ickowicz, A., Manlay, R. J., Bernoux, M., and Vayssières, J.: Livestock induces strong spatial heterogeneity of soil  $\text{CO}_2$ ,  $\text{N}_2\text{O}$ ,  $\text{CH}_4$  emissions within a semi-arid sylvo-pastoral landscape in West Africa, *J. Arid Land*, 9, 201–221, <https://doi.org/10.1007/s40333-017-0001-y>, 2017.
- Austin, A. T., Yahdjian, L., Stark, J. M., Belnap, J., Porporato, A., Norton, U., Ravetta, D. A., and Schaeffer, S. M.: Water pulses and biogeochemical cycles in arid and semi-arid ecosystems, *Oecologia*, 141, 221–235, 2004.
- Bachelet D., Hunt, H. W., and Detling J. K. A: simulation model of intraseasonal carbon and nitrogen dynamics of blue grama swards as influenced by above-ground and belowground grazing, *Ecol. Model.*, 44, 231–252, 1989.
- Bai E., Li, S., Xu, W., Li, W., Dai W., and Jiang, P.: A meta-analysis of experimental warming effects on terrestrial nitrogen pools and dynamics, *New Phytol.*, 199, 441–451, 2013.
- Bobbink, R., Hicks, K., Galloway, J., Spranger, T., Alkemade, R., Ashmore, M., Cinderby, S., Davidson, E., Dentener, F., Emmett, B., Erisman, J., Fenn, M., Nordin, A., Pardo, L., Vries, W. De, Hicks, K., Galloway, J., Bobbink, R., Davidson, E., Dentener, F., Cinderby, S., Spranger, T., and Bustamante, M.: Global assessment of nitrogen deposition effects on terrestrial plant diversity, *Ecol. Appl.*, 20, 30–59, <https://doi.org/10.1890/08-1140.1>, 2010.
- Breman, H. and de Ridder, N.: Manuel sur les pâturages des pays sahéliens, DLO, Centre de Recherches Agrobiologiques, Wageningen, 567 pp., 1991.
- Borken, W. and Matzner, E.: Reappraisal of drying and wetting effects on C and N mineralization and fluxes in soils, *Glob. Change Biol.*, 15, 808–824, 2009.
- Butterbach-Bahl, K., Stange, F., Papen, H., and Li, C.: Regional inventory of nitric oxide and nitrous oxide emissions for forest soils of southeast Germany using the biogeochemical model PnET-N-DNDC, *J. Geophys. Res.*, 106, 34155–34166, 2001.
- Butterbach-Bahl, K., Kahl, M., Mykhayliv, L., Werner, C., Kiese, R., and Li, C.: A European-wide inventory of soil NO emissions using the biogeochemical models DNDC/Forest-DNDC, *Atmos. Environ.*, 43, 1392–1402, 2009.
- Camillo, P. J. and Gurney, R. J.: A resistance parameter for bare soil evaporation models, *Soil Sci.*, 141, 95–105, 1986.
- Casenave, A. and Valentin, C.: Les états de surface de la zone sahélienne: influence sur l’infiltration, de l’ORSTOM, 229 pp., 1990.
- Chen, W., Zheng, X., Chen, Q., Wolf, B., Butterbach-Bahl, K., Brüggemann, N., and Lin, S.: Effects of increasing precipitation and nitrogen deposition on  $\text{CH}_4$  and  $\text{N}_2\text{O}$  fluxes and ecosystem respiration in a degraded steppe in Inner Mongolia, China, *Geoderma* 192, 335–340, 2013.
- Choudhury, B. J. and Monteith, J. L.: A four-layer model for the heat budget of homogeneous land surfaces, *Q. J. R. Meteor. Soc.*, 11, 373–398, 1988.
- Conrad, R.: Soil microorganisms as controllers of atmospheric trace gases ( $\text{H}_2$ ,  $\text{CO}$ ,  $\text{CH}_4$ ,  $\text{OCS}$ ,  $\text{N}_2\text{O}$ , and  $\text{NO}$ ), *Microbiol. Rev.*, 60, 609–640, 1996.
- De Bruin, B., Penning de Vries, F. W. T., Van Broekhoven, L. W., Vertregt, N., and Van de Geijn, S. C.: Net mineralization, nitrification and  $\text{CO}_2$  production in alternating moisture conditions in an unfertilized low humus sandy soil from the Sahel, *Plant Soil*, 113, 69–78, 1989.
- Delgado-Baquerizo, M., Maestre, F. T., Gallardo, A., Bowker, M. A., Wallenstein, M. D., Quero, J. L., Ochoa, V., Gozalo, B., García-Gómez, M., Soliveres, S., García-Palacios, P., Berdugo, M., Valencia, E., Escolar, C., Arredondo, T., Barraza-Zepeda, C., Bran, D., Carreira, J. A., Chaieb, M., Conceição, A. A., Derak, M., Eldridge, D. J., Escudero, A., Espinosa, C.I., Gaitán, J., Gabriel Gatica, M., Gómez-González, S., Guzman, E., Gutierrez, J. R., Florentino, A., Hepper, E., Hernández, R. M., Huber-Sannwald, E., Jankju, M., Liu, J., Mau, R. L., Miriti, M., Monerri, J., Naseri, K., Noumi, Z., Polo, V., Prina, A., Pucheta, E., Ramírez, E., Ramírez-Collantes, D. A., Romão, R., Tighe, M.,

- Torres, D., Torres-Díaz, C., Ungar, E.D., Val, J., Wamiti, W., Wang D., and Zaady, E.: Decoupling of soil nutrient cycles as a function of aridity in global drylands, *Nature*, 502, 672–676, <https://doi.org/10.1038/nature12670>, 2013.
- Delon, C., Serça, D., Boissard, C., Dupont, R., Dutot, A., Laville, de Rosnay, P., and Delmas, R.: Soil NO emissions modelling using artificial neural network, *Tellus B*, 59, 502–513, 2007.
- Delon, C., Galy-Lacaux, C., Boone, A., Lioussé, C., Serça, D., Adon, M., Diop, B., Akpo, A., Lavenue, F., Mougin, E., and Timouk, F.: Atmospheric nitrogen budget in Sahelian dry savannas, *Atmos. Chem. Phys.*, 10, 2691–2708, <https://doi.org/10.5194/acp-10-2691-2010>, 2010.
- Delon, C., Galy-Lacaux, C., Adon, M., Lioussé, C., Serça, D., Diop, B., and Akpo, A.: Nitrogen compounds emission and deposition in West African ecosystems: comparison between wet and dry savanna, *Biogeosciences*, 9, 385–402, <https://doi.org/10.5194/bg-9-385-2012>, 2012.
- Delon, C., Mougin, E., Serça, D., Grippa, M., Hiernaux, P., Diawara, M., Galy-Lacaux, C., and Kergoat, L.: Modelling the effect of soil moisture and organic matter degradation on biogenic NO emissions from soils in Sahel rangeland (Mali), *Biogeosciences*, 12, 3253–3272, <https://doi.org/10.5194/bg-12-3253-2015>, 2015.
- Delon, C., Galy-Lacaux, C., Serça, D., Loubet, B., Camara, N., Gardrat, E., Saneh, I., Fensholt, R., Tagesson, T., Le Dantec, V., Sambou, B., Diop, C., and Mougin, E.: Soil and vegetation-atmosphere exchange of NO, NH<sub>3</sub>, and N<sub>2</sub>O from field measurements in a semi-arid grazed ecosystem in Senegal, *Atmos. Environ.*, 156, 36–51, 2017.
- Diawara, M.: Impact de la variabilité climatique au nord Sahel (Gourma) sur la dynamique des ressources pastorales et leurs conséquences sur les productions animales (Ph.D. thesis), Toulouse Univ., 150 p., 2015.
- Diawara, M., Hiernaux, P., Mougin, E., Grippa, M., Delon, C., and Diakité, H. S.: Effets de la pâture sur la dynamique de la végétation herbacée au Sahel (Gourma, Mali): une approche par modélisation, *Cahiers de l'Agriculture*, 27, 15010, <https://doi.org/10.1051/cagri/2018002>, 2018.
- Elberling B., Fensholt, R., Larsen, L., Petersen A.-I. S., and Sandholt, I.: Water content and land use history controlling soil CO<sub>2</sub> respiration and carbon stock in savanna soil and groundnut fields in semi-arid Senegal, *Geogr. Tidsskr.*, 103, 47–56, <https://doi.org/10.1080/00167223.2003.10649491>, 2003.
- Farquhar, G. D., Firth, P. M., Wetselaar, R., and Weir, B.: On the gaseous exchange of ammonia between leaves and the environment: determination of the ammonia compensation point, *Plant Physiol.*, 66, 710–714, 1980.
- Flechar, C. R. and Fowler, D.: Atmospheric ammonia at a moorland site. II: Long-term surface-atmosphere micrometeorological flux measurements, *Q. J. R. Meteor. Soc. A*, 124, 759–791, 1998.
- Flechar, C. R., Massad, R.-S., Loubet, B., Personne, E., Simpson, D., Bash, J. O., Cooter, E. J., Nemitz, E., and Sutton, M. A.: Advances in understanding, models and parameterizations of biosphere-atmosphere ammonia exchange, *Biogeosciences*, 10, 5183–5225, <https://doi.org/10.5194/bg-10-5183-2013>, 2013.
- Ford, D. J., Cookson, W. R., Adams, M. A., and Grierson, P. F.: Role of soil drying in nitrogen mineralization and microbial community function in semi-arid grasslands of north-west Australia, *Soil Biol. Biochem.*, 39, 1557–1569, 2007.
- Fowler, D., Steadman, C. E., Stevenson, D., Coyle, M., Rees, R. M., Skiba, U. M., Sutton, M. A., Cape, J. N., Dore, A. J., Vieno, M., Simpson, D., Zaehle, S., Stocker, B. D., Rinaldi, M., Facchini, M. C., Flechar, C. R., Nemitz, E., Twigg, M., Erisman, J. W., Butterbach-Bahl, K., and Galloway, J. N.: Effects of global change during the 21st century on the nitrogen cycle, *Atmos. Chem. Phys.*, 15, 13849–13893, <https://doi.org/10.5194/acp-15-13849-2015>, 2015.
- Gritsch, C., Egger, F., Zehetner, F., and Zechmeister-Boltenstern, S.: The effect of temperature and moisture on trace gas emissions from deciduous and coniferous leaf litter, *J. Geophys. Res.-Biogeo.*, 121, 1339–1351, <https://doi.org/10.1002/2015JG003223>, 2016.
- Hanan, N., Boulain, N., Williams, C., Scholes, R., and Archibald, S.: Functional convergence in ecosystem carbon exchange in adjacent savanna vegetation types of the Kruger National Park, South Africa, in: Hill, M. J. and Hanan, N., *Ecosystem Function in Savannas*, CRC Press, Boca Raton, 57–76, 2011.
- Hanan, N., Kabat, P., Dolman, J., and Elbers, J. A. N.: Photosynthesis and carbon balance of a Sahelian fallow savanna, *Glob. Change Biol.*, 4, 523–538, 1998.
- Harms, T. K. and Grimm, N. B.: Responses of trace gases to hydrologic pulses in desert floodplains, *J. Geophys. Res.*, 117, G01035, <https://doi.org/10.1029/2011JG001775>, 2012.
- Hiernaux, P., Fernandez-Rivera, S., Schlecht, E., Turner, M. D., and Williams, T. O.: Livestock-mediated nutrient transfers in Sahelian agro-ecosystems, edited by: Renard, G., Neef, A., Becker, K., and von Oppen, M., *Soil fertility management in West African land use systems*, Niamey, Niger, 4-8.03.97, Margraf Verlag, Weikersheim, Germany, 339–347, 1998.
- Hiernaux, P. and Turner, M. D.: The influence of farmer and pastoralism management practices on desertification processes in the Sahel, in: *Global desertification: do humans cause deserts?* edited by: Reynolds, J. F. and Stafford Smith, D. M., Dahlem University Press, Berlin, 135–148, 2002.
- Homyak, P. M. Sickman J. O.: Influence of soil moisture on the seasonality of nitric oxide emissions from chaparral soils, Sierra Nevada, California, USA, *J. Arid Environ.*, 103, 46–52, 2014.
- Homyak, P. M., Kamiyama, M., Sickman, J. O., and Schimel, J. P.: Acidity and organic matter promote abiotic nitric oxide production in drying soils, *Glob. Change Biol.*, <https://doi.org/10.1111/gcb.13507>, 2016.
- Hudman, R. C., Moore, N. E., Mebust, A. K., Martin, R. V., Russell, A. R., Valin, L. C., and Cohen, R. C.: Steps towards a mechanistic model of global soil nitric oxide emissions: implementation and space based-constraints, *Atmos. Chem. Phys.*, 12, 7779–7795, <https://doi.org/10.5194/acp-12-7779-2012>, 2012.
- Jaeglé, L., Martin, R. V., Chance, K., Steinberger, L., Kurosu, T. P., Jacob, D. J., Modi, A. I., Yoboué, V., Sighe-Nkamdjou, L., and Galy-Lacaux, C.: Satellite mapping of rain-induced nitric oxide emissions from soils, *J. Geophys. Res.*, 109, D21310, <https://doi.org/10.1029/2003JD004406>, 2004.
- Jia, B., Zhou, G., Wang, Y., Wang, F., and Wang, X.: Effects of temperature and soil water-content on soil respiration of grazed and ungrazed *Leymus chinensis* steppes, Inner Mongolia, *J. Arid Environ.*, 67, 60–76, 2006.
- Jones, H. G.: *Plants and Microclimate, A Quantitative Approach to Environmental Plant Physiology*, 2nd Edn., Cambridge University Press, Cambridge, 428 pp., 1992.

- Körner, C. H., Scheel, J. A., and Bauer, H.: Maximum leaf diffusive conductance in vascular plants, *Photosynthetica*, 13, 45–82, 1979.
- Krul, J. M., Penning de Vries, F. W. T., and Traore, K.: Les processus du bilan d'azote, in "La productivité des pâturages sahéliens", Eds Penning De Vries FWT and Traoré F, Wageningen, 226–246, 1982.
- Laouali D., Galy-Lacaux, C., Diop, B., Delon, C., Orange, D., Lacaux, J. P., Akpo, A., Lavenu, F., Gardrat, E., and Castera, P.: Long term monitoring of the chemical composition of precipitation and wet deposition fluxes over three Sahelian savannas, *Atmos. Environ.*, 50, 314–327, 2012.
- LI-COR Biosciences: EDDYPRO Eddy Covariance Software Version 4.0 User's Guide and Reference, LI-COR Inc., Lincoln, 200 pp., 2012.
- Liu, K. and Crowley, D.: Nitrogen deposition effects on carbon storage and fungal: bacterial ratios in coastal sage scrub soils of southern California, *J. Env. Qual.*, 38, 2267–2272, 2009.
- Lloyd, J. and Taylor, J. A.: On the temperature dependence of soil respiration, *Funct. Ecol.*, 8, 315–323, 1994.
- Loubet, B., Decuq, C., Personne, E., Massad, R. S., Flechard, C., Fanucci, O., Mascher, N., Gueudet, J.-C., Masson, S., Durand, B., Genermont, S., Fauvel, Y., and Cellier, P.: Investigating the stomatal, cuticular and soil ammonia fluxes over a growing tritical crop under high acidic loads, *Biogeosciences*, 9, 1537–1552, <https://doi.org/10.5194/bg-9-1537-2012>, 2012.
- Loubet, B., Carozzi, M., Voylokov, P., Cohan, J.-P., Trochard, R., and Générmont, S.: Evaluation of a new inference method for estimating ammonia volatilisation from multiple agronomic plots, *Biogeosciences*, 15, 3439–3460, <https://doi.org/10.5194/bg-15-3439-2018>, 2018.
- Manabe, S.: Climate and the Ocean circulation: 1. The atmospheric circulation and the hydrology of the earth's surface, *Mon. Weather Rev.*, 97, 739–774, 1969.
- Massad, R.-S., Nemitz, E., and Sutton, M. A.: Review and parameterisation of bi-directional ammonia exchange between vegetation and the atmosphere, *Atmos. Chem. Phys.*, 10, 10359–10386, <https://doi.org/10.5194/acp-10-10359-2010>, 2010.
- McCalley, C. K. and Sparks, J. P.: Controls over nitric oxide and ammonia emissions from Mojave Desert soils, *Oecologia*, 156, 871–881, 2008.
- McCree, K. J.: An equation for the rate of respiration of white clover plants grown under controlled conditions, in *Prediction and Measurements of Photosynthetic Productivity*, edited by: Setlik, I., Pudoc, Wageningen, 221–229, 1970.
- Medinets, S., Skiba, U., Rennenberg, H., and Butterbach-Bahl, K.: A review of soil NO transformation: Associated processes and possible physiological significance on organisms, *Soil Biol. Biochem.*, 80, 92–117, 2015.
- Meixner, T. and Fenn, M.: Biogeochemical budgets in a Mediterranean catchment with high rates of atmospheric N deposition – importance of scale and temporal asynchrony, *Biogeochemistry*, 70, 331–356, 2004.
- Monteith, J. L.: Evaporation and environment in state and movement of water in living organisms (19th symposium of the society for Experimental Biology), UK, Cambridge University Press, 205–234, 1965.
- Monteith, J. L. and Unsworth, M. H.: *Principles of Environmental Physics*, Edward Arnold, London, p. 291, 1990.
- Moorhead, D. L. and Reynolds, J. F.: A general model of litter decomposition in the northern Chihuahuan desert, *Ecol. Modell.*, 56, 197–219, 1991.
- Mougin, E., Lo Seen D., Rambal S., Gaston A., and Hiernaux P.: A Regional Sahelian Grassland Model To Be Coupled with Multi-spectral Satellite Data, I: Model Description and Validation, *Remote Sens. Environ.*, 52, 181–193, 1995.
- Nemitz, E., Milford, C., and Sutton, M. A.: A two-layer canopy compensation point model for describing bi-directional biosphere/atmosphere exchange of ammonia, *Q. J. Roy. Meteor. Soc.*, 127, 815–833, 2001.
- Nouvellon, Y., Rambal S., Lo Seen D., Moran M. S., Lhomme J.P., Bégué A., Chehbouni A. G., and Kerr, Y.: Modelling of daily fluxes of water and carbon from shortgrass steppes, *Agr. Forest Meteorol.*, 100, 137–153, 2000.
- Parton, W. J.: Predicting soil temperatures in a shortgrass steppe, *Soil Sci.*, 138, 93–101, 1984.
- Penning de Vries, F. W. T. and Djitéye, M. A.: La productivité des pâturages sahéliens, Une étude des sols, des végétations et de l'exploitation de cette ressource naturelle, *Agr. Res. Rep.*, 918, Pudoc, Wageningen, 525 pp., 1982.
- Perroni-Ventura, Y., Montaña, C., and García-Oliva, F.: Carbon-nitrogen interactions in fertility island soil from a tropical semi-arid ecosystem, *Funct. Ecol.*, 24, 233–242, <https://doi.org/10.1111/j.1365-2435.2009.01610.x>, 2010.
- Personne, E., Loubet, B., Herrmann, B., Mattsson, M., Schjoerring, J. K., Nemitz, E., Sutton, M. A., and Cellier, P.: SURFATM-NH3: a model combining the surface energy balance and bi-directional exchanges of ammonia applied at the field scale, *Biogeosciences*, 6, 1371–1388, <https://doi.org/10.5194/bg-6-1371-2009>, 2009.
- Pilegaard, K.: Processes regulating nitric oxide emissions from soils, *Phil. Trans. R. Soc. B*, 368, 20130126, <https://doi.org/10.1098/rstb.2013.0126>, 2013.
- Potter, C. S., Matson, P.A., Vitousek, P.M., and Davidson, E.A.: Process modeling of controls on nitrogen trace gas emissions from soils worldwide, *J. Geophys. Res.*, 101, 1361–1377, 1996.
- Pumpanen, J., Kolari, P., Ilvesniemi, H., Minkinen, K., Vesala, T., Niinistö, S., Lohila, A., Larmola, T., Morero, M., Pihlatie, M., Janssens, I., Curiel Yuste, J., Grünzweig, J.M., Reth, S., Subke, J.-A., Savage, K., Kutsch W., Østreng, G., Ziegler, W., Anthoni, P., Lindroth, A., and Hari, P.: Comparison of different chamber techniques for measuring soil CO<sub>2</sub> efflux, *Agr. Forest Meteorol.*, 123, 159–176, 2004.
- Rambal, S. and Cornet, A.: Simulation de l'utilisation de l'eau et de la production végétale d'une phytocénose sahélienne du Sénégal, *Acta Oecol.-Oec. Plant*, 3, 381–397, 1982.
- Reichstein, M., Falge, E., Baldocchi, D., Papale, D., Aubinet, M., Berbigier, P., Bernhofer, C., Buchmann, N., Gilmanov, T., Granier, A., Grunwald, T., Havrankova, K., Ilvesniemi, H., Janous, D., Knohl, A., Laurila, T., Lohila, A., Loustau, D., Matteucci, G., Meyers, T., Miglietta, F., Ourcival, J. M., Pumpanen, J., Rambal, S., Rotenberg, E., Sanz, M., Tenhunen, J., Seufert, G., Vaccari, F., Vesala, T., Yakir D., and Valentini, R.: On the separation of net ecosystem exchange into assimilation and ecosystem respiration: review and improved algorithm, *Glob. Change Biol.*, 11, 1424–1439, 2005.
- Riddick, S. N., Blackall, T. D., Dragosits, U., Daunt, F., Braban, C. F., Tang, Y. S., MacFarlane, W., Taylor, S., Wanless, S., and

- Sutton, M. A.: Measurement of ammonia emissions from tropical seabird colonies, *Atmos. Environ.*, 89, 35–42, 2014.
- Riddick, S. N., Blackall, T. D., Dragosits, U., Daunt, F., Newell, M., Braban, C. F., Tang, Y. S., Schmale, J., Hill, P. W., Wanless, S., Trathan, P., and Sutton, M. A.: Measurement of ammonia emissions from temperate and sub-polar seabird colonies, *Atmos. Environ.*, 134, 40–50, 2016.
- Saugier, B.: Transport de CO<sub>2</sub> et de vapeur d’eau à l’interface végétation-atmosphère. Thèse Docteur d’Etat, Université des Sciences et Techniques du Languedoc, Montpellier, 156 pp., 1974.
- Saxton, K. E., Rawls, W. J., Romberger, J. S., and Papendick, R. I.: Estimating generalized soil-water characteristics from texture, *Soil Sci. Soc. Am. J.*, 50, 1031–1036, 1986.
- Schlecht, E. and Hiernaux, P.: Beyond adding up inputs and puts: process assessment and upscaling in modelling nutrient flows, *Nutr. Cy. Agroecosys.*, 70, 303–319, 2004.
- Schlesinger, W. H. and Peterjoh, W. T.: Processes controlling ammonia volatilization from Chihuahuan desert soils, *Soil Biol. Biochem.*, 23, 637–642, 1991.
- Shen, W., Jenerette, G. D., Hui, D., and Scott, R. L.: Precipitation legacy effects on dryland ecosystem carbon fluxes: direction, magnitude and biogeochemical carryovers, *Biogeosciences*, 13, 425–439, <https://doi.org/10.5194/bg-13-425-2016>, 2016.
- Sutton, M. A., Schjørring, J. K., and Wyers, G. P.: Plant atmosphere exchange of ammonia, *Phil. T. R. Soc. London A*, 351, 261–276, 1995.
- Sutton, M. A., Reis, S., Riddick, S. N., Dragosits, U., Nemitz, E., Theobald, M. R., Sim Tang, Y., Braban, C. F., Vieno, M., Dore, A. J., Mitchell, R. F., Wanless, S., Daunt, F., Fowler, D., Blackall, T. D., Milford, C., Flechard, C. R., Loubet, B., Massad, R., Cellier, P., Personne, E., Coheur, P. F., Clarisse, L., Van Damme, M., Ngadi, Y., Clerbaux, C., Ambelas Skjøth, C., Geels, C., Hertel, O., Wichink Kruit, R. J., Pinder, R. W., Bash, J. O., Walker, J. T., Simpson, D., Horváth, L., Misselbrook, T. H., Bleeker, A., Dentener, F., and de Vries, W.: Towards a climate-dependent paradigm of ammonia emission and deposition, *Phil. T. R. Soc. B*, 368, 20130166, <https://doi.org/10.1098/rstb.2013.0166>, 2013.
- Tagesson, T. and Lindroth, A.: High soil carbon efflux rates in several ecosystems in southern Sweden, *Boreal Environ. Res.*, 12, 65–80, 2007.
- Tagesson, T., Fensholt, R., Cropley, F., Guiro, I., Horion, S., Ehammer, and A., Ardö, J.: Dynamics in carbon exchange fluxes for a grazed semi-arid savanna ecosystem in West Africa, *Agr. Ecosyst. Environ.*, 205, 15–24, 2015a.
- Tagesson, T., Fensholt, R., Guiro, I., Rasmussen, M. O., Huber, S., Mbow, C., Garcia, M., Horion, S., Sandholt, I., Holm-Rasmussen, B., Götsche, F. M., Ridler, M.-E., Olén, N., Olsen, J. L., Ehammer, A., Madsen, M., Olesen, F. S., and Ardö, J.: Ecosystem properties of semi-arid savanna grassland in West Africa and its relationship to environmental variability, *Glob. Change Biol.*, 21, 250–264, 2015b.
- Tagesson, T., Fensholt, R., Cappelaere, B., Mougin, E., Horion, S., Kergoat, L., Nieto, H., Mbow, C., Ehammer, A., Demarty, J., and Ardö, J.: Spatiotemporal variability in carbon exchange fluxes across the Sahel, *Agr. Forest Meteorol.*, 226/227, 108–118, 2016a.
- Tagesson, T., Ardö, J., Guiro, I., Cropley, F., Mbow, C., Horion, S., Ehammer, A., Mougin, E., Delon, C., Galy-Lacaux, C., and Fensholt, R.: Very high CO<sub>2</sub> exchange fluxes at the peak of the rainy season in a West African grazed semi-arid savanna ecosystem, *Geogr. Tidsskr.*, 116, 93–109, <https://doi.org/10.1080/00167223.2016.1178072>, 2016b.
- Thornley, J. H. M. and Cannell, M. G. R.: Modelling the components of plant respiration: Representation and realism, *Ann. Bot.*, 85, 937–937, 2000.
- Van Keulen, H.: Simulation of water use and herbage growth in arid regions, *Simulation Monographs*, Pudoc, Wageningen, 176 pp., 1975.
- Vinken, G. C. M., Boersma, K. F., Maasakkers, J. D., Adon, M., and Martin, R. V.: Worldwide biogenic soil NO<sub>x</sub> emissions inferred from OMI NO<sub>2</sub> observations, *Atmos. Chem. Phys.*, 14, 10363–10381, <https://doi.org/10.5194/acp-14-10363-2014>, 2014.
- Wang, L., Manzoni, S., Ravi, S., Riveros-Iregui, D., and Caylor, K.: Dynamic interactions of ecohydrological and biogeochemical processes in water-limited systems, *Ecosphere*, 6, 133, <https://doi.org/10.1890/ES15-00122.1>, 2015.
- Wichink Kruit, R. J., van Pul, W. A. J., Otjes, R. P., Hofschreuder, P., Jacobs, A. F. G., and Holtslag, A. A. M.: Ammonia fluxes and derived canopy compensation points over non-fertilized agricultural grassland in the Netherlands using the new gradient ammonia – high accuracy – monitor (GRAHAM), *Atmos. Environ.*, 41, 1275–1287, 2007.
- Xu, X., Tian, H., and Hui, D.: Convergence in the relationship of CO<sub>2</sub> and N<sub>2</sub>O exchanges between soil and atmosphere within terrestrial ecosystems, *Glob. Change Biol.*, 14, 1651–1660, <https://doi.org/10.1111/j.1365-2486.2008.01595.x>, 2008.
- Xu, M. and Shang, H.: Contribution of soil respiration to the global carbon equation, *J. Plant Physiol.*, 203, 16–28, 2016.
- Yan, X., Ohara, T., and Akimoto, H.: Statistical modelling of global soil NO<sub>x</sub> emissions, *Global Biogeochem. Cy.*, 19, GB3019, <https://doi.org/10.1029/2004GB002276>, 2005.
- Yienger, J. J. and Levy II, H.: Empirical model of global soil biogenic NO<sub>x</sub> emissions, *J. Geophys. Res.*, 100, 11447–11464, 1995.
- Zhang, L., Brook, J. R., and Vet, R.: A revised parameterization for gaseous dry deposition in air-quality models, *Atmos. Chem. Phys.*, 3, 2067–2082, <https://doi.org/10.5194/acp-3-2067-2003>, 2003.
- Zhang, L., Wright, P. L., and Asman, W. A. H.: Bi-directional air surface exchange of atmospheric ammonia – A review of measurements and a development of a big-leaf model for applications in regional-scale air-quality models, *J. Geophys. Res.*, 115, D20310, <https://doi.org/10.1029/2009JD013589>, 2010.
- Zörner, J., Penning de Vries, M., Beirle, S., Sihler, H., Veres, P. R., Williams, J., and Wagner, T.: Multi-satellite sensor study on precipitation-induced emission pulses of NO<sub>x</sub> from soils in semi-arid ecosystems, *Atmos. Chem. Phys.*, 16, 9457–9487, <https://doi.org/10.5194/acp-16-9457-2016>, 2016.